JOURNAL OF GEOPHYSICAL RESEARCH, VOL. 107, NO. D8, 4061, 10.1029/2001JD000670, 2002

Tropical snowline depression at the Last Glacial Maximum: Comparison with proxy records using a single-cell tropical climate model

Arthur M. Greene, Richard Seager, and Wallace S. Broecker
Lamont-Doherty Earth Observatory of Columbia University, Palisades, New York, USA

Received 26 March 2001; revised 11 July 2001; accepted 15 August 2001; published 19 April 2002.

[1] The substantial lowering of tropical snowlines at the Last Glacial Maximum (LGM), circa 21 kya, is examined using a modified version of the single-cell tropical climate model of *Betts and Ridgway* [1989]. These authors concluded that it was difficult to reconcile the large depression of snowlines at the LGM with the small reduction in mean tropical sea-surface temperature (SST) of the Climate: Long-Range Investigation, Mapping, and Prediction (CLIMAP) reconstruction. Here, climatic implications of the snowline depression are compared, not with CLIMAP, but with temperature proxies ($\delta^{18}O$ and Sr/Ca ratios in corals, noble gas concentrations in aquifers, alkenone and Mg/Ca ratios in deep-sea sediments and recent faunal reconstructions) whose LGM values have been interpreted as implying lower surface temperatures in the tropics. It proves difficult, in the framework of this model, to reconcile the coldest of the indicated paleotemperatures with the observed snowline depression, which by itself is found to be consistent with an SST reduction of $\sim$3 K. A cooling of this magnitude corresponds most closely to recent warm-pool LGM sea-surface temperature estimates based on Mg/Ca paleothermometry. Discordance among the various proxy reconstructions may result, at least in part, from regional variations in surface temperature change at the LGM. *INDEX TERMS:* 3309 Meteorology and Atmospheric Dynamics: Climatology (1620); 3344 Meteorology and Atmospheric Dynamics: Paleoclimatology; 3307 Meteorology and Atmospheric Dynamics: Boundary layer processes; 3374 Meteorology and Atmospheric Dynamics: tropical meteorology; *KEYWORDS:* Paleoclimatology, climatology, boundary layer processes, tropical meteorology, glaciology, snow and ice

1. Introduction

[2] The depression of tropical snowlines at the Last Glacial Maximum (LGM) has not yet been definitively reconciled with sea-surface temperature (SST) reconstructions. Notable among such reconstructions was that of the *Climate: Long-Range Investigation, Mapping, and Prediction (CLIMAP) Project Members* [1981], which was based on faunal assemblages and indicated a mean tropical SST reduction of $\sim$1 K at the LGM. The relatively warm tropical SSTs of the CLIMAP reconstruction were questioned by *Rind and Peteet* [1985] as well as *Betts and Ridgway* [1992] and more recently have been tested by the Paleoclimate Model Intercomparison Project (PMIP) [*Pinot et al.*, 1999]. The Rind and Peteet study, as well as the PMIP simulations, utilized general circulation models (GCMs) and found that the small SST reductions postulated by CLIMAP were incompatible with terrestrial records of LGM temperature change, including pollen, vegetation, and snowline shifts, that indicated greater cooling. The Betts and Ridgway study, employing a single-cell budget model of the tropical circulation, focused only on the thermodynamical implications of the observed snowline depression, in the context of an atmospheric temperature profile controlled by boundary layer interactions over the tropical oceans. This study reached a similar conclusion.

[3] Since CLIMAP, other temperature proxies have been developed, among them $\delta^{18}O$ and Sr/Ca ratios in corals [*Beck et al.*, 1985; *Guilderson et al.*, 1994], noble gas concentrations in aquifers [*Stute et al.*, 1995; *Weyhenmeyer et al.*, 2000], alkenones [*Bard et al.*, 1997; *Bard*, 1999; *Emeis et al.*, 1995; *Lyle et al.*, 1992; *Ohkouchi et al.*, 1994; *Rostek et al.*, 1993; *Sikes and Keigwin*, 1994; *Sonzogni et al.*, 1998], and Mg/Ca ratios in pelagic sediments [*Hastings et al.*, 1998; *Lea et al.*, 2000]. In addition, new estimates based on faunal assemblages have been produced [*Mix et al.*, 1999; *Lee and Slowey*, 1999]. The LGM surface temperature depressions inferred from these records range from 1.5 to 6.5 K. It should be noted that groundwater records are indicators of terrestrial temperatures, changes in which may be decoupled to some degree from SST changes of even proximal ocean regions [*Weyhenmeyer et al.*, 2000]. However, since we shall argue that a reduction in tropical SST of 5 K or more is too great to be consistent with the observed snowline depressions, some offset of land surface temperature changes from those in SST may serve to ameliorate the apparent discordance between these indicators.

[4] In this study we employ *Betts and Ridgway*'s [1989] single-cell tropical climate model, hereinafter referred to as BR89, as modified by *Seager et al.* [2000], in order to investigate the sensitivity of snowline elevations to changes in SST, surface winds, above-inversion moisture, and autoconversion efficiency in the shallow cumulus clouds that populate the tropical marine atmospheric boundary layer. The effects of LGM precipitation changes on snowlines are considered as well, using a regression relationship derived from the modern distribution of snowlines as well as temperature and precipitation fields.

[5] In section 2 we provide an overview of the conceptual framework of this study, which is followed in section 3 by a more detailed model description. Sections 4 and 5 provide further discussion of key theoretical assumptions, while section 6 considers the role of precipitation in forcing snowline variations. Section 7 discusses boundary layer changes required at the LGM, and section 8, the core of the paper, describes sensitivity experiments in which the model parameter space is explored. In section 9 we discuss the

0148-0227/02/2001JD000670$09.00

implications of these experiments, and in section 10 we discuss possible sources of error. Section 11 provides comparisons with the various proxy records, while section 12 discusses the effects of drizzle, one feature that sets the present model apart from its predecessor. A summary is provided in section 13. Finally, in Appendix A, we describe the regression calculations.

2. Conceptual Framework

[6] The study employs a one-dimensional model of the tropical climate, as identified above. It is a radiative-convective equilibrium model, meaning that it seeks a state in which the thermal and moisture structure of the modeled atmospheric column is in equilibrium with the radiation field, as well as with the heat and water fluxes from the ocean surface, subject to specified boundary conditions. The model is "semiempirical," in that it imposes a general atmospheric structure, including a composite boundary layer, that is rooted in observations [*Betts and Ridgway*, 1989]. Structurally, we believe it to be basic enough to be equally applicable to both modern and LGM tropical climates. Since the model has only a single spatial dimension (in the vertical), the various model parameters, including SST, surface fluxes, temperature, and moisture at a given height as well as the imposed boundary conditions, can each assume only a single equilibrium value. These are taken to represent spatially averaged quantities.

[7] Deep convection, occurring in the west Pacific warm pool and other areas, proceeds along a characteristic vertical temperature profile. This profile, which is effectively communicated throughout the tropics, is determined by properties of the low-level, or mixed-layer, air converging into the convective regions. The model does not represent the precise locations where convection is actually occurring, which occupy only a small percentage of the area of the tropics at any one time. Instead, it simulates the subsiding regions, in which mixed-layer air is conditioned as it converges toward the zones where deep convection occurs. Although the modeled area is specified only in climatic terms, it can initially be thought of as representing an average taken over the subsiding areas of the warm pool.

[8] To constrain the relationship between snowline elevation, temperature, and precipitation, a series of regression calculations was carried out, utilizing modern distributions of glacier equilibrium-line altitudes (ELAs) and climate variables. The regression relationship enables a quantitative estimate of the effect of LGM precipitation change on snowlines.

[9] The core of the paper consists of a suite of sensitivity experiments, in which the parameter space of the model is explored. The object of these experiments is to delineate a likely range for SST reduction at the LGM, given the atmospheric freezing height depression implied by the observed lowering of snowlines, and taking into account possible variations in precipitation.

3. Model Description

[10] The climate model employed consists of a single column and represents the subsiding regions of the warm pool, in the sense that SST is taken to be close to that in the areas where deep convection occurs. The model balances the budgets of heat and moisture for the mixed layer, convective boundary layer (CBL), and troposphere as a whole. A radiation module accounts for ozone, carbon dioxide (CO_2), and water vapor as well as the effects of boundary layer clouds. The fractional area occupied by these clouds is specified, and the radiative perturbation due to high-level clouds is assumed to equal the atmospheric export of heat from the tropics, as in BR89. The net radiative cooling of the troposphere is then balanced by the sensible and (principally) latent heat fluxes from the ocean surface. In the steady state solutions found by the model, radiative cooling of the troposphere is also equal to the subsidence warming; this provides a constraint on the subsidence term in the CBL heat budget. SST is computed by requiring that the net surface heat flux be equal to the specified ocean heat transport.

[11] The model convective boundary layer consists of two sublayers, the uppermost of which is fractionally populated by the above mentioned clouds. Below this is a nearly well-mixed sublayer, which extends to the ocean surface (the 2 mbar surface layer of BR89 is omitted in this model version). The vertical profiles of potential temperature and moisture within the CBL are parameterized via a saturation point mixing line [*Betts*, 1982, 1985], with air near the ocean surface and that above the inversion constituting the two end-members. Above the CBL a moist, or moist virtual, adiabatic temperature structure is assumed, corresponding to the equivalent potential temperature, θ_e, of the subcloud layer.

[12] The moisture structure above the CBL is determined as in BR89. First, air just above the inversion, or CBL top, is assumed to have a specific humidity corresponding to saturation near the atmospheric freezing level at the corresponding model pressure. The precise temperature at which saturation specific humidity is computed is a tunable parameter, which we vary in the experiments to be described. Next, specific humidity at the tropopause is specified by choosing a value for subsaturation at this level, subsaturation being defined as the difference between saturation and actual pressure levels. Thus a subsaturation value of -30 mbar would imply that a parcel would become just saturated, with respect to water vapor, if raised 30 mbar. Finally, the tropospheric moisture profile is derived by linear interpolation of the subsaturation, between the above-inversion and tropopause values.

[13] An important difference between the present model and the original formulation of BR89 is the incorporation of drizzle. The drizzle parameterization used follows that of *Albrecht* [1993] and was first incorporated by *Seager et al.* [2000] into a two-cell version of the Betts-Ridgway model. Allowing the CBL clouds to drizzle produces a more realistic representation of boundary layer depth (along with corresponding changes in other model diagnostics) than does a model with only nonprecipitating clouds. Figure 1 shows the modeled cloud top pressure with and without drizzle over a range of SSTs. Without precipitation, cloud top pressure varies from $\sim$815 mbar at an SST of 295 K to 700 mbar at 305 K. When a modest amount of drizzle is permitted (0.25–0.75 mm/d for the plot shown), the corresponding variation in cloud top pressure is $\sim$830–790 mbar. Thus the inclusion of drizzle lowers the inversion height and damps the response of inversion pressure level to rising SST. *Schubert et al.* [1995] have shown that a similar effect can be induced by large-scale dynamical processes, which cannot be represented explicitly in a single-cell model. In the parameterization used, the drizzle rate is proportional to precipitable water in the cloud layer, which increases as the layer deepens. Drizzle lowers the inversion level by removing cloud liquid water that would otherwise be available for evaporative cooling [*Albrecht*, 1993]. The removal of liquid water also reduces cloud optical depth and albedo, with corresponding effects on the surface radiation budget.

[14] In the LGM experiments to be described, oceanic heat export and other parameters are varied, and the model returns the corresponding equilibrium SST, along with various other diagnostics. In the next section we discuss the relationship of atmospheric freezing height to a key parameter returned by the model. More detailed descriptions of the basic and revised versions of the model are given by BR89, *Clement and Seager* [1999], and *Seager et al.* [2000].

4. Significance of Subcloud θ_e

[15] Most important for our purposes, among the diagnostics returned by the model, are SST and the equivalent potential temperature, θ_e, of the subcloud, or atmospheric mixed layer. The

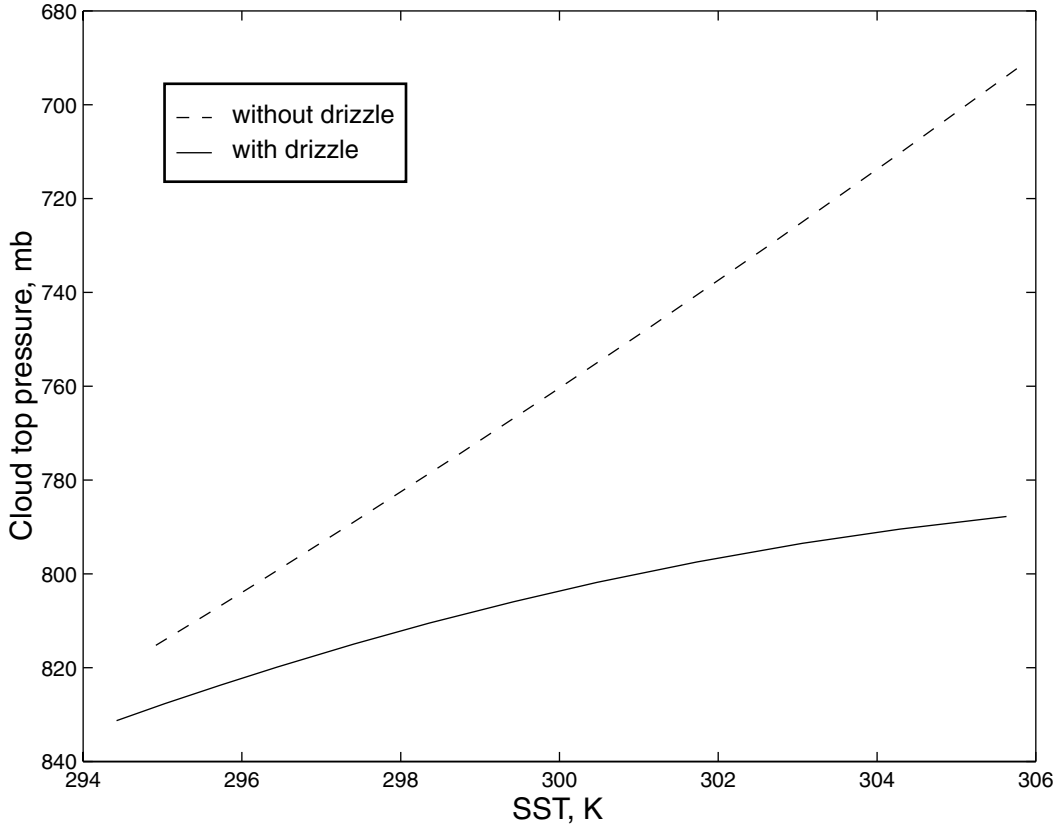

Figure 1. Cloud top pressure with and without drizzle. As SST increases, cloud top rises, but less rapidly in the case where drizzle is permitted.

temperature profile set by deep convection is assumed to follow an adiabat corresponding to this θ_e [*Emanuel*, 1994], because such convection originates near the surface and because, by definition, θ_e is conserved by convectively rising parcels. Because of the inability of the low-latitude atmosphere to support large horizontal temperature gradients [*Held and Hou*, 1980; *Schneider*, 1977], the vertical temperature profile thus produced, the moist adiabat, prevails rather uniformly throughout the tropics (Figure 2). Thus it is the subcloud θ_e, rather than SST per se, that determines the near-uniform height of the freezing isotherm in the tropical atmosphere, and, as we shall see, to a large extent the elevation of snowlines.

[16] There is evidence that the observed tropical temperature profile is actually slightly cooler, or less stable, than the moist adiabat [*Betts*, 1982; *Xu and Emanuel*, 1989], and indeed, some degree of tropospheric instability must accumulate in order for deep convection to occur. To first order, radiative cooling tends to destabilize the tropical atmosphere, while deep convection acts to restore stability. The net effect of these competing processes is an intermediate temperature profile, with the relative influences of radiation and convection being inversely proportional to their respective adjustment timescales [*Emanuel*, 1994]. These timescales ($\sim$1 day for convective but an order of magnitude more for radiative adjustment) are such that the resulting temperature profile is close to, but slightly cooler than, the moist adiabat. We do not model the adjustment process explicitly but attempt to achieve a similar result by employing as a reference profile the moist virtual adiabat, the neutral temperature profile with respect to reversible ascent of saturated parcels. "Reversible ascent," in this context, implies retention of condensed water, at least as high as the freezing level. The concomitant buoyancy loading causes parcels to reach a given temperature at a lower elevation than if the water had been rained out and produces a temperature profile that apparently corresponds to observations more closely than the classical moist adiabat [*Betts*, 1982].

5. Lapse Rate Assumptions

[17] The temperature profile produced by deep convection differs markedly from the constant lapse rate often invoked in considering the relationship of surface temperature changes to shifts in the freezing height, as illustrated in Figure 3. The plots in Figure 3 are constructed so that the height of the modern freezing level, $\sim$4900 m, corresponds to observations. The LGM freezing level is depressed by 780 m, which equals the observed snowline depression [*Porter*, 2001] minus the LGM reduction in sea level. Modern surface air temperature is taken as 300 K.

[18] In Figure 3a, a constant lapse rate of 5.5°/km is used; Figure 3b, on the other hand, employs fixed values of θ_e: 349.4 K (modern) and 337 K (LGM). Profiles in Figure 3b are moist virtual adiabats corresponding to these θ_e values, as discussed in section 4. These profiles are not simply offset, but have somewhat different shapes. In Figure 3b, cloud base, or the lifting condensation level, was taken 60 mbar above the surface for both modern and LGM profiles. In the constant-lapse-rate scenario a reduction in SST of 4.3 K is required to produce the observed freezing-level depression; for the scenario in which a constant θ_e is assumed, the required surface temperature reduction is only 3.1 K. The precise difference produced by such computations depends on a number of boundary layer parameters, but clearly the choice of lapse rate assumption can

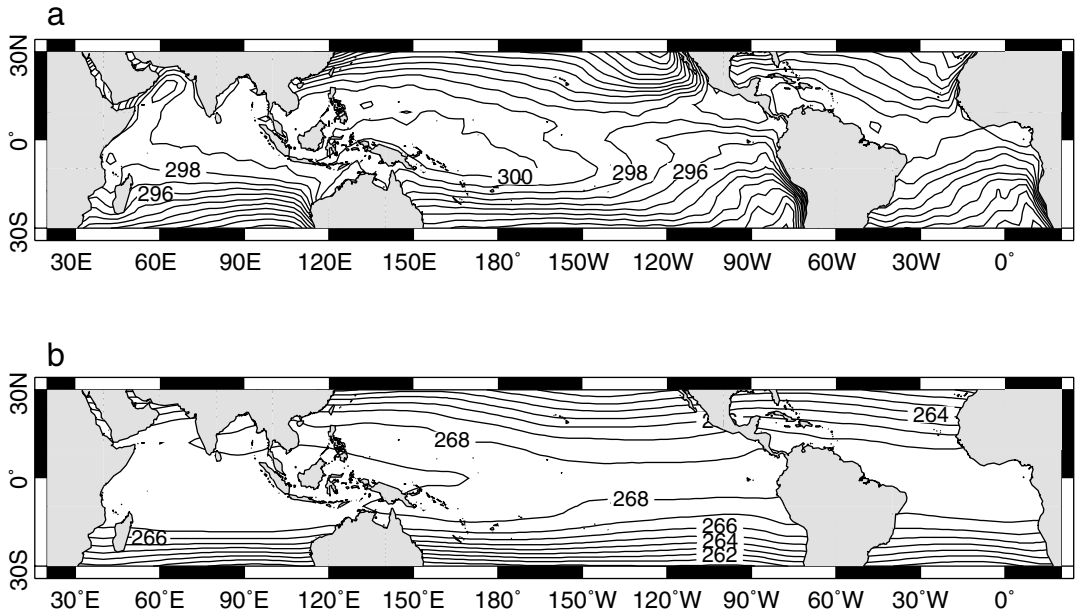

Figure 2. Contrast between tropical midtropospheric temperatures and those near the surface. (a) Climatology of the 1000 mbar temperature, ~100 m above the sea surface. The high degree of structure suggests strong coupling to SST. (b) Climatology for the 500 mbar temperature, ~6000 m above the surface. At this level the temperature pattern is considerably smoother. Data come from the NCEP-NCAR reanalysis for the years 1951–1980 [*Kalnay et al.*, 1996].

make a significant difference in the SST change inferred from a given shift in the atmospheric freezing level.

6. Effect of Precipitation Changes

[19] To constrain the relationship between snowlines, height of the atmospheric freezing isotherm, and precipitation, a multiple regression analysis was conducted (see Appendix A for details). This analysis yielded the following relationship for tropical sites:

$$\mathrm{ELA} = 537 + 1.01\mathrm{FH} - 0.51\mathrm{PA}, \qquad (1)$$

where ELA is the glacier equilibrium-line altitude, or snowline, FH is the annually averaged freezing height, and PA is the annual precipitation (ELA and FH are given here in meters; PA is given in millimeters). The mean annual precipitation for these sites is 1084 mm/yr (values are derived from gridded data), so the regression relation implies that a 20% reduction in precipitation would raise snowlines by ~100 m relative to the atmospheric freezing height. Alternately, to hold snowlines at a constant level while precipitation decreases by 20%, a compensating reduction in freezing height of 100 m would be required. Increases in precipitation would have corresponding effects, but of opposite sign.

[20] While the regression relationship above could theoretically be used to predict ELA shifts for individual glaciers in the tropics, given regional changes in FH and PA, we do not consider sites individually in this study. Essentially, this is because our model is one-dimensional and is only intended to represent spatially averaged values. However, there is a corollary benefit to this averaging: the reduced statistical uncertainty involved in predicting the mean response.

7. Required θ_e Shift for the Observed Snowline Depression

[21] Table 1 lists parameters for a model base state representative of the recent climate, for which the tropical atmospheric freezing isotherm lies near 4900 m. The specified ocean heat export, 23.8 W/m^2, is within the range of estimates presented by *Trenberth and Caron* [2001], and the boundary layer cloud fraction of 26% is consistent with surface observations as described by *Warren et al.* [1988]. The base state SST, 301.5 K, is near but not quite as high as core warm-pool values, which range above 302 K. The value for surface wind speed, 5 m/s, was chosen to be somewhat lower than the 6.7 m/s used by *Betts and Ridgway* [1992] for their modern climate, while the SST was chosen to be higher than their base state value of 300 K [*Betts and Ridgway*, 1992]. One might think of these choices as specifying a modeled region that is more representative of the subsiding areas of the warm pool, rather than of the tropics as a whole. However, the conclusions of this study are not sensitive to these choices.

[22] Since sea level was ~120 m lower at the LGM [*Fairbanks*, 1989; *Fleming et al.*, 1998] and the absolute snowline depression averaged 900 m [*Porter*, 2001], the mean snowline depression, relative to the lowered sea level of the LGM, would have been 780 m. The computed moist virtual adiabatic temperature profile has a freezing height response, $\partial z_0/\partial\theta_e = 63$ m/K, so this snowline shift would require a reduction in θ_e of 12.4 K, from 349.4 to 337 K, were it due solely to changes in the freezing height. A 20% reduction in precipitation, using the regression relation derived above, would decrease the required θ_e by 1.6 K, to 335.4 K, with a corresponding reduction in SST. Thus, for a given snowline depression a drier climate would correspond to a cooler sea surface, since it would necessitate a larger SST reduction for the same snowline shift. This observation has been made before [see, e.g., *Rind*, 1990], at least in the qualitative sense.

[23] From a budget perspective we would expect a colder climate to have a less intense hydrological cycle, i.e., lower average precipitation, owing to the reduced longwave cooling of the atmosphere, and the concomitant reduction of balancing latent heat flux from the ocean surface. The modeled latent heat flux decreases by ~11% for a reduction in SST of 3 K and 16% for a reduction of 5 K. Thus, for the contemplated range of temperature changes a precipitation reduction of 20% would represent a large excursion with respect to the computed model budgets.

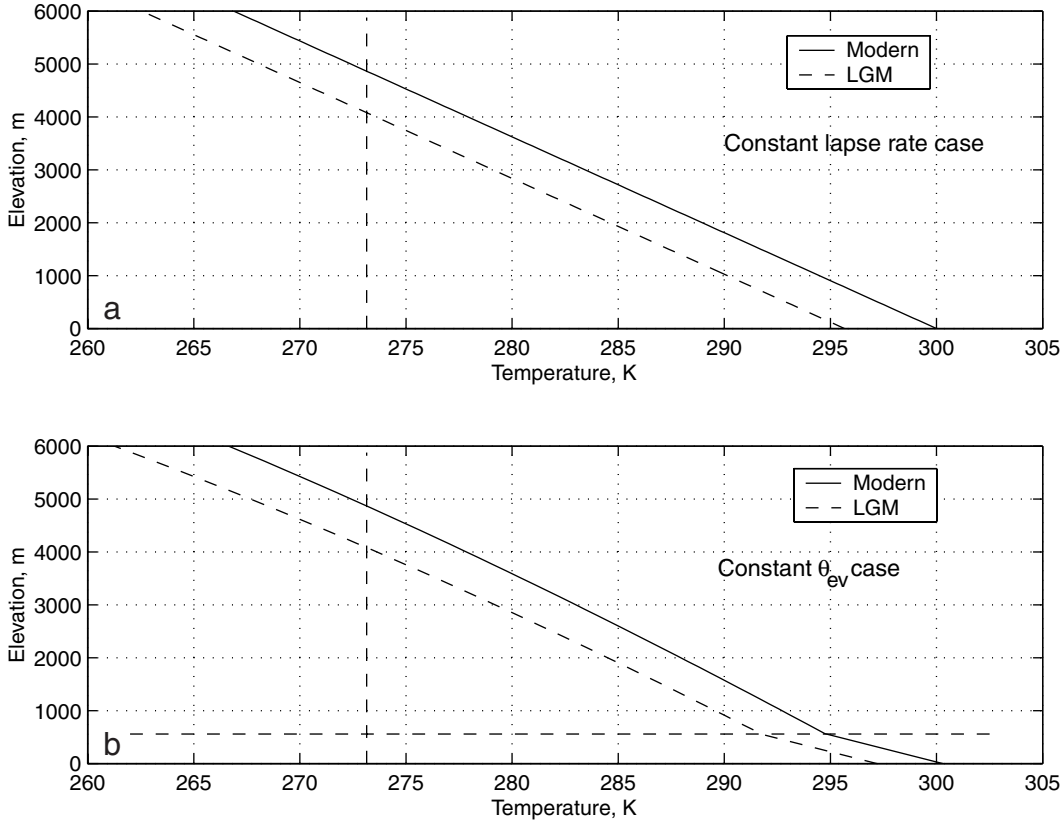

Figure 3. Modern-to-LGM reduction in freezing height under two scenarios: (a) constant lapse rate and (b) constant θ_{ev}. The freezing temperature is indicated by a vertical dashed line, and the modern and LGM profiles as solid and dashed lines, respectively. On the lower plot, the horizontal dashed line shows the level of cloud base, where the lapse rate changes from dry to moist adiabatic.

[24] Given the limited spatial sampling implied by the geographical distribution of snowline data in the tropics, it cannot be assumed with certainty that average precipitation change at the sites of glaciers was strictly proportional to changes in the surface latent heat flux. This matter is discussed further in section 9.

8. Sensitivity Experiments

[25] In the following experiments we explore the model parameter space by varying boundary conditions as well as internal parameters. We seek a state in which the atmospheric mixed-layer θ_e lies at 337 K (335.4 K), corresponding to a scenario in which there is no change (a 20% reduction) in precipitation. The precipitation referred to would be the LGM analog of the gridded precipitation field used to derive the regression relation, as described in Appendix A. We vary the specified ocean heat export, boundary layer cloud fraction, autoconversion of cloud liquid water into precipitation, surface wind speed, and a parameter, T_{sl}, that controls above-inversion specific humidity. Each of these variables may have a significant effect on the tropical climate.

Table 1. Model Base State

Parameter	Value
Sea level pressure	1012 mbar
SST	301.5 K
Surface wind speed	5 m/s
Cloud fraction	0.26
Ocean heat export	23.8 W/m^2
CO_2 concentration	330 ppm
Subcloud θ_e	349.4 K
Freezing level	4870 m

[26] In all experiments, atmospheric CO_2 was reduced to 180 ppm and sea level pressure (SLP) was increased to 1026 mbar, reflecting the lowered sea level of the LGM [*Guilderson et al.*, 1994; *Fleming et al.*, 1998] and the corresponding redistribution of atmospheric mass due to the presence of large continental ice sheets [*Betts and Ridgway*, 1992]. Reduction of CO_2 lowers the equilibrium SST, while increasing SLP has the opposite effect in this model. The sensitivities are such that the equilibrium SST is shifted upward by ~0.5 K in going from modern to LGM values of CO_2 and SLP. In the following experiments, reductions in equilibrium SST are computed using the base state value, 301.5 K, as a starting point.

[27] Figure 4 shows the results of typical experiments. In each panel, oceanic heat export and a single other parameter were varied, as indicated on the plot axes. Contours for three values of equilibrium SST, 300.5, 298.5, and 296.5 K, representing temperature reductions, relative to the base state value, of 1, 3, and 5 K, respectively, are shown These are labeled with the SST reduction represented, rather than the absolute SST. Also plotted are θ_e contours at 10 K intervals as well as a contour for the target θ_e value of 337 K, which is shown as a thick dashed line.

[28] Although the changes in ocean heat export needed to produce the required SST reductions may appear to be rather large in some plots, these transports are simply standing in, in these experiments, for the assortment of altered boundary conditions that may have brought about the lowered sea-surface temperatures of the LGM. We do not attempt to diagnose here a complete picture of

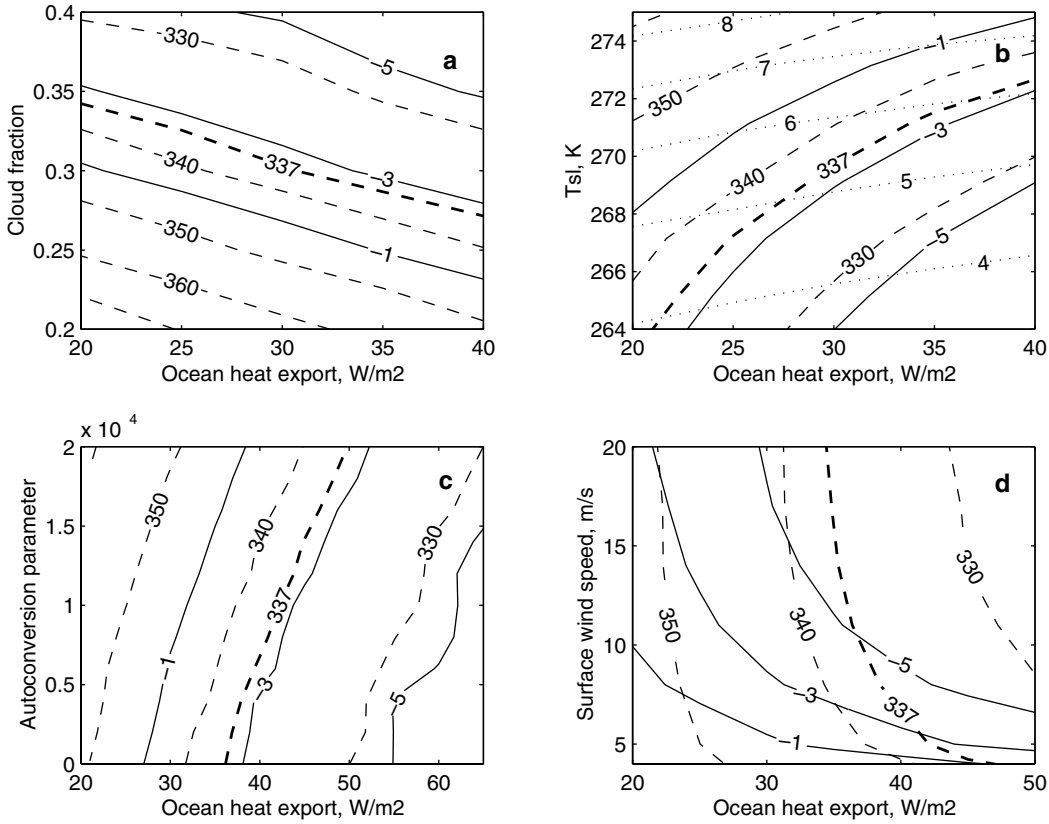

Figure 4. Results of typical experiments. Ocean heat export increases along the *x* axis; the *y* axes show variations of four different model parameters. Contours of SST and atmospheric mixed-layer θ_e (solid and dashed lines, respectively) show the response of these variables to variations of the imposed boundary conditions. Three contours are shown for SST, representing reductions of 1, 3, and 5 K relative to the base state, and labeled accordingly. The "criterion" value for θ_e of 337 K, corresponding to the constant-precipitation scenario, is plotted with a thick dashed line. The *y* axis variables are (a) cloud fraction (dimensionless), (b) T_{sl}, an internal parameter controlling the above-inversion specific humidity, expressed in K (Contours of the above-inversion specific humidity have been added in this panel and are shown as dotted lines labeled with single-digit values. Units in this case are g/kg.), (c) the autoconversion, or rainout efficiency parameter (dimensionless), and (d) surface wind speed, in m/s. Note that *x* axis limits are not the same in every plot.

the altered boundary conditions that may have prevailed at the LGM.

[29] In Figure 4a the *y* variable is boundary layer cloud fraction. The principal effect of increasing the cloud fraction is to reduce the net surface solar radiation, owing to the high cloud albedo (typically 0.6, compared with 0.07 for the ocean surface). The model sensitivity is sufficient to lower equilibrium SST by 3 K as cloud fraction goes from 0.26 to 0.35. Values of θ_e are seen to decrease in step with SST, as indicated by the parallel appearance of the respective contours; the SST reduction corresponding to the target θ_e is somewhat less than 3 K. The required reduction in SST is seen to be independent of any joint variations of cloud fraction and oceanic heat export.

[30] The *y* axis of Figure 4b shows the internal parameter T_{sl}, discussed in section 3. T_{sl} controls the above-inversion specific humidity q_t according to $q_t = q_s(\theta_{es}, T_{sl})$, where θ_{es} is the saturation equivalent potential temperature corresponding to the mixed-layer θ_e computed by the model, q_s is saturation specific humidity, and T_{sl} is a temperature near the freezing point. Contours of q_t have been added in this plot and are shown as dotted lines with single-digit labels. The above-inversion humidity is seen to increase with T_{sl}, as do the equilibrium SST and θ_e, reflecting shifts in the longwave radiation budget. Water vapor above the inversion absorbs upwelling longwave radiation and reradiates a portion back downward, requiring higher values of both equilibrium SST and mixed-layer θ_e. The coupling of SST and θ_e is also apparent in this plot, with the SST reduction corresponding to the target θ_e value again seen to be slightly less than 3 K.

[31] In Figure 4c the autoconversion parameter, which controls the fraction of cloud liquid water that is removed as precipitation, appears on the *y* axis. As noted above, drizzle removes liquid water from the cloud layer (the droplet size distribution remains unchanged) and reduces both cloud optical depth and albedo, raising the equilibrium SST. Subcloud θ_e also changes in step with SST in this plot, and the required SST reduction is similar to that in Figures 4a and 4b. Joint variations in autoconversion and ocean heat export do not appear to influence the strong coupling of SST and subcloud θ_e and, by inference, the coupling between SST and snowline elevation.

[32] The model sensitivity of mixed-layer θ_e to SST change, $\partial\theta_e/\partial$SST, equals 4.36 (at an SST of 300 K). Thus the reduction in θ_e of 12.4 K that we seek could be obtained with a reduction in SST of 2.8 K. In fact, the strong coupling of SST and mixed-layer θ_e observed in the plots so far examined, as shown by their parallel contours, effectively specifies the SST reduction corresponding to a given snowline depression, even as the other parameters so far explored are allowed to change. For example, an SST reduction of 5 K would lower θ_e by 21.8 K and snowlines by 1370 m. This is considerably greater than the 780 m target

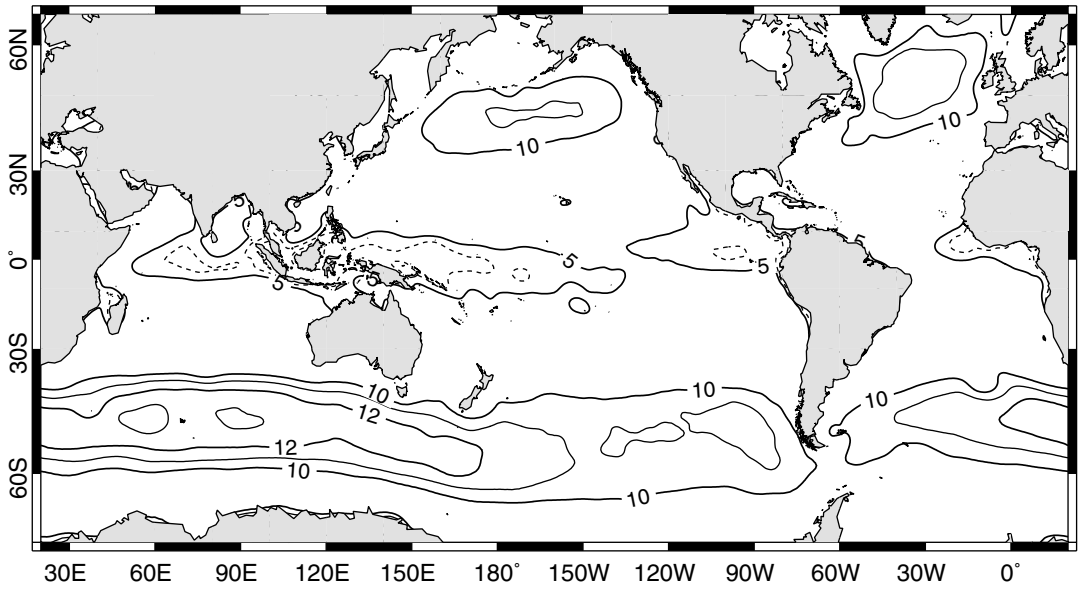

Figure 5. Mean annual scalar wind speed, 1980–1989, from *Trenberth et al.* [1989]. Only those areas with wind speeds <5 m/s (dotted contours) or >10 m/s (solid contours) are shown. Contour interval is 1 m/s.

value and well outside the uncertainty of 39 m in the estimated mean snowline depression. Thus, unless a process exists that can modify the coupling between θ_e and SST, a cooling of 2.8 K (3.2 K for the reduced precipitation scenario) would be both necessary and sufficient to account for the LGM snowline lowering.

[33] Freezing height changes more rapidly with θ_e along the moist adiabat, with a sensitivity of 71 m/K at 300 K (these sensitivities vary slowly with temperature). If the moist adiabat were adopted as the reference profile, the required change in θ_e would be 11 K. The SST change required would then be 2.5 K (with no precipitation change) or 2.8 K (with a 20% reduction in precipitation).

[34] Figure 4d differs from the other panels in Figure 4, in that the contours of SST and θ_e are not everywhere parallel. As surface wind speed increases, the latent and sensible heat fluxes from the ocean surface also increase, lowering the equilibrium SST. But the consequent moistening and heating of the mixed-layer air above the sea surface retard the depression of its θ_e, relative to the lowering of the underlying SST. The differing sensitivities of SST and θ_e, indicated by the difference in slopes of the SST and θ_e contours, indicate that variations in wind speed can induce SST changes that are independent to some degree of changes in the mixed-layer θ_e, and thus from the snowline elevation. For instance, we see that the snowline lowering would be consistent with a 5 K reduction in SST if mean LGM wind speed had increased to 11 m/s. In general, for a given snowline depression, increased surface wind speeds would be consistent with lower LGM SSTs and vice versa. Specifying a likely range for LGM SST thus becomes, at least in part, a question of defining a corresponding likely range of surface wind speed over the convecting regions during glacial times.

[35] Today, wind speeds above 10 m/s are more characteristic of the midlatitude oceans than the regions of deep convection, where winds tend to be <5 m/s [*Trenberth et al.*, 1989] (Figure 5). The global distribution of SST is negatively skewed [*Wallace*, 1992], with the convecting regions, namely, the warm pool, occupying a relatively large area having small SST gradients and correspondingly light winds [*Lindzen and Nigam*, 1987]. It is difficult to make a conclusive case for the existence of a similar SST distribution at the LGM, but a modicum of circumstantial evidence may be cited that tends to support this view. The CLIMAP LGM SST field, the only global reconstruction to date, does show extended regions of uniform SST that are similar in location to today's warm pool, if somewhat different in configuration in the February and August reconstructions. *Farrera et al.* [1999], in a recent, comprehensive survey, find that terrestrial evidence supports the existence of these spatial patterns, even though the evidence also indicates that average CLIMAP SSTs are somewhat too high. The recent SST reconstruction of *Mix et al.* [1999] is limited to the Atlantic and eastern Pacific and would not modify the LGM "warm pool" areas greatly. It is often assumed that the LGM must have been a time of increased temperature gradients and commensurately stronger winds. However, *Rind* [1998], in a study comparing proxy records with model simulations, found that in a colder climate, weaker temperature gradients were indicated in low latitudes, while stronger gradients may have prevailed at high latitudes.

[36] We do not claim by these observations to have conclusively demonstrated the immutability of winds in the convecting areas of the tropics. But taken together with the rather large wind speed changes that would be required to shift the SST-θ_e coupling by an appreciable amount, these observations at least render the idea of small LGM wind speed changes a plausible one.

9. Discussion

[37] Modest changes in cloud fraction, perhaps coupled with increased oceanic heat export, are sufficient to reduce glacial-age SST to values consistent with any of the paleotemperature proxy records discussed. However, the tight coupling between SST and θ_e, the equivalent potential temperature of subcloud air in the marine atmospheric boundary layer, restricts the plausible range of SST reduction once a value for the snowline depression is known. This is the case because it is the subcloud θ_e that determines the temperature structure of the tropical atmosphere, and thus the elevation of snowlines. The single model parameter capable of modifying the consequent close coupling of SST and snowline elevation is surface wind speed. While the global wind field in a glacial climate may well have differed from that of modern times,

at least some evidence suggests that wind speeds may not have been too different in the ocean areas of greatest significance for snowline elevations. These are the regions of deep convection, where the lightest winds prevail.

[38] In the case of a drier climate, a lower SST would be indicated, since the required freezing level depression would exceed the lowering of snowlines. A reduction in precipitation of 20% would, in this manner, lower the required θ_e by 1.6 K and the SST by 0.4 K for a total LGM SST reduction of 3.2 K. As noted in section 7, an equilibrium state with a lower SST has a correspondingly reduced surface latent heat flux, the presumed source of this precipitation, with an SST reduction of 5 K corresponding to a 16% reduction in the latent heat flux. An iterative procedure applied to the SST–latent heat–snowline shift–SST loop arrives at an SST reduction of 3.0 K, with a corresponding latent heat flux reduction of ~10% and a snowline rise, relative to the freezing level, of 50 m. Thus an SST reduction of 3.0 K and a precipitation reduction of 10% would be consistent with the model latent heat budget as well as the observed snowline depression. *Farrera et al.* [1999] note that terrestrial evidence supports the notion of general tropical aridity at the LGM.

[39] The assumption that changes in the surface latent heat budget must be accompanied by proportional changes in the high mountain snows that drive glacier fluctuations is, of course, open to question. Actual precipitation change at the LGM seems to have been quite variable, with areas of wet and dry climates in close proximity. For example, *Thompson et al.* [1998] report wetter LGM conditions at Sajama (18°S) in the Bolivian Andes, in accord with Altiplano lake-level studies [e.g., *Baker et al.*, 2000]. However, *Thompson et al.* [1995] report drier LGM conditions at Huascarán (9°S) in Peru. In other studies, *Seltzer et al.* [2000] found that hydrological fluctuations between the northern and southern tropics were antiphased (during the last glacial-interglacial transition), while *Gasse* [2000] notes that tropical east Africa was arid at the LGM, Lake Victoria having completely vanished at this time. Aside from these indications of variability, there is also the question of sampling, since glaciated areas in the tropics are highly localized. Thus, even if average tropical precipitation had been reduced in precisely the same proportion as the surface latent heat flux, there is no assurance that this reduction would be mirrored by the average precipitation received in the areas in which LGM snowline depressions were recorded. The fact that our regression relationship was derived using gridded, and therefore spatially averaged, data ameliorates this situation, but only to a limited extent. Thus, although a reduction in mean tropical precipitation may be consistent with a reduced flux of latent heat from the ocean surface, such a reduction need not have applied to the area sampled by the observed glaciers.

[40] Finally, snowline depression among the sample glaciers was fairly uniform (Table 3). Taken together with the spatial homogeneity of midtropospheric temperatures, this suggests that the component of ELA variation forced by changes in precipitation must have been small compared to the component forced by temperature change. If these roles were reversed, one would expect to see a much larger range of snowline variations, presumably of both signs, given the apparently high spatial variability of LGM precipitation changes. This is not observed. Thus it is likely that precipitation played a secondary role in forcing snowline changes at the LGM.

[41] It is interesting that *Hostetler and Clark* [2000] arrived at a very similar value for warm-pool SST depression, albeit by a totally different route. In their study a mass-balance model, in conjunction with a high-resolution digital elevation map, was used to process output from a GCM. By adjusting local temperatures, but retaining the GCM-derived precipitation field, the mass-balance model was tuned until a set of simulated glaciers attained LGM configurations consistent with those inferred from geomorphic evidence. ELA values were then determined from the computed mass balance profiles and related to the SST field used as a model boundary condition. LGM cooling in the warm pool area was estimated as 3 K in this study.

10. Sources of Error

[42] Sources of error may reside in the basic assumptions employed, in the model physics, in the determination of the snowline depression itself, in the estimate of sea level lowering at the LGM, and possibly other factors. Many of these uncertainties are difficult to quantify, but some estimates may provide a context in which to consider the computed SST depressions.

[43] The sample standard deviation associated with the snowline lowering itself is given by *Porter* [2001] as 135 m. With a sample size of 12, the standard error of the mean would be 39 m, corresponding to an uncertainty of 0.14 K in the SST reduction, given the sensitivities discussed above.

[44] As mentioned, changes in the high mountain precipitation that drives glacier mass balance, and ultimately the adjustment of snowlines to changes in climate state, may not have been strictly proportional to changes in the surface latent heat flux. For an uncertainty of 10% in LGM precipitation averaged over the tropical glacier sites used in the regression calculation (and with an implied precipitation variable similar to the gridded field utilized in the regression), the corresponding uncertainty in LGM SST change would be 0.18 K.

[45] It is difficult to rule out modest changes in mean wind speeds in the convecting areas, although a case was made earlier that large changes do not seem likely. The model sensitivities are such that an uncertainty in the change in wind speed of 0.5 m/s, or 10%, corresponds to an uncertainty in the required SST depression of 0.4 K, keeping θ_e constant at 337 K, i.e., consistent with the observed snowline shift.

[46] These error figures, while providing useful information, do not constitute a complete description of the uncertainty associated with the computed SST reduction. In addition to potential sources of error which remain unaddressed, the possible covariation of error sources, such as winds and mountain precipitation, is not explored here.

11. Comparison to SST Proxy Reconstructions

[47] In section 7 the SST reduction required to account for the observed snowline depression, given no change in precipitation, was given as 2.8 K, while in section 9 an estimate of 3.0 K was suggested on the basis of a presumed consistency between modeled latent heat flux and assumed precipitation changes. On the other hand, had precipitation been 10% greater at the LGM, the corresponding SST reduction would have been 2.6 K. Paleothermometry based on alkenones indicates LGM SST depressions of ~2 K [*Bard*, 1999], somewhat closer to the CLIMAP value; measurements of noble gas concentrations in groundwater yield estimates of surface air temperature reduction of 5–6.5 K [*Stute et al.*, 1995; *Weyhenmeyer et al.*, 2000]. Sr/Ca and $\delta^{18}O$ records from Barbados corals suggest a 5 K cooling [*Guilderson et al.*, 1994], while the warm-pool SST depression derived from Mg/Ca paleothermometry is 2.8 K. Recent faunal-based estimates yield a cooling of 2 K near Hawaii [*Lee and Slowey*, 1999] and as much as 5–6 K in the eastern equatorial Pacific and equatorial Atlantic oceans [*Mix et al.*, 1999].

[48] Figure 6 shows the locations to which a number of these proxy records, as well as the cited snowline data [*Porter*, 2001], correspond. These data are also listed in Tables 2 (proxy data) and 3 (snowlines). The proxy records cited are intended to be representative of the range of extant reconstructions, rather than an exhaustive tabulation. *Crowley* [2000] discusses potential problems associated with a number of these indicators. However, since we

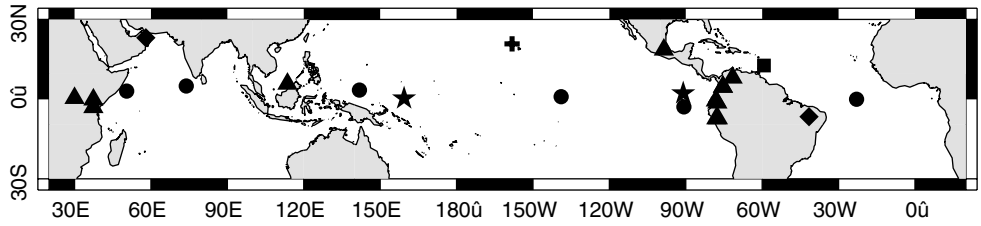

Figure 6. Sites corresponding to proxy SST reconstructions and snowline data locations: triangles, snowline data; square, the single LGM coral record; diamonds, noble gas records; circles, alkenone data; stars, Mg/Ca records; cross, a faunal estimate. The temperature fields reconstructed by *Mix et al.* [1999] in the eastern equatorial Pacific and equatorial Atlantic are not shown. Additional data exist for some of the listed proxies, particularly alkenones.

focus here on the implications of the snowline depression, we simply take the various proxy estimates at face value and compare them as they stand with inferences from the model sensitivity tests.

[49] From a purely numerical point of view, the model estimates presented here would appear to be in closest agreement with SST depressions derived from Mg/Ca paleothermometry, although the uncertainties are not so small as to conclude that alkenone-derived estimates are incompatible with model results. We use the qualifier ''numerical'' to emphasize that the model estimates are assumed to represent SST changes in the regions of deep convection, as discussed earlier. Thus, depending on location, other proxy records may indeed be quite compatible with the model estimates from a dynamical point of view.

[50] The SST estimates of *Mix et al.* [1999], which apply to the equatorial eastern Pacific and Atlantic, reinforce this point. The reconstructions are fields, rather than point estimates, and the degree of cooling indicated ranges up to 6 K. As indicated in section 8, an SST reduction of this magnitude would appear to be too large to support the observed snowline depression. The regions of cooling, however, are far from the warm-pool area and would therefore not be expected to dominate the atmospheric temperature response.

[51] However, in an atmospheric general circulation model simulation of the LGM climate, in which the eastern Pacific and Atlantic SST fields of *Mix et al.* [1999] were combined with CLIMAP SSTs elsewhere, *Hostetler and Mix* [1999] found east African and Andean snowline depressions to be in better accord with observations than when the pure CLIMAP SST field was was used. This suggests that strict consideration of warm-pool SSTs alone may represent something of an oversimplification and that temperatures (and θ_e values) in other convecting regions may also play a role in determining freezing height in the tropics. For the purposes of the present study this idea could be assimilated by simply redefining the modeled area to represent some average taken over the various convective zones. Such an average might be weighted to account for the relative importance of the different areas represented.

[52] Two proxy records represent locations near the center of the present warm-pool area: the Mg/Ca record of *Lea et al.* [2000] and the alkenone record of *Ohkouchi et al.* [1994]; owing to their locations, these records might be given somewhat more weight than the others, for the purposes of the comparison at hand. The alkenone record indicates an LGM cooling $\leq$1.5 K; for Mg/Ca the estimated cooling is 2.8 K.

12. Drizzle

[53] It can be seen from Figure 4c that variations in the autoconversion parameter do not noticeably alter the parallel character of SST and θ_e contours. Thus the elimination of drizzle would not be expected to greatly affect the snowline-SST dependence on which the estimates given above are based. A series of model runs using nonprecipitating clouds confirms this expectation. These experiments indicate that the sensitivity of θ_e to SST changes, $\partial\theta_e/\partial$SST, is reduced from 4.36 to 4.24, leading to estimated SST shifts $\sim$0.1 K greater than those for experiments in which the effects of drizzle are included. Thus the inclusion of drizzle has only a very minor effect on the numerical conclusions presented.

[54] The possible dependence of cloud fraction on autoconversion parameter, or rainout efficiency, is not developed here; in the model runs, each must be specified independently. Since drizzle depletes liquid water, the substance of which the clouds in question are formed, it is likely that such a dependence exists [*Albrecht*, 1989]. However, the SST-θ_e coupling does not seem to depend on changes in either cloud fraction or autoconversion. Identification of a link between them may thus be more relevant for an understanding

Table 2. SST Proxy Records Referred to in the Text[a]

Proxy Type	Latitude,[b] deg	Longitude,[c] deg	SST Reduction, K	Source
Coral Sr/Ca, δ^{18}O	13.2	−59.3	5.0	*Guilderson et al.* [1994]
Noble gas	−7.0	−41.5	5.4±0.6	*Stute et al.* [1995]
Noble gas	23.5	58.0	6.5±0.6	*Weyhenmeyer et al.* [2000]
Alkenone	5.1	73.9	2.5±0.3	*Rostek et al.* [1993]
Alkenone	3.5	141.9	$\leq$1.5	*Ohkouchi et al.* [1994]
Alkenone	3.2	50.4	1.5±0.7	*Bard et al.* [1997]
Alkenone	1.0	−139.0	0.5±0.4	*Lyle et al.* [1992]
Alkenone	0.0	−23.0	1.8±0.6	*Sikes and Keigwin* [1994]
Alkenone	−3.1	90.9	0.0±0.15	*Emeis et al.* [1995]
Mg/Ca	0.3	159.4	2.8±0.7	*Lea et al.* [2000]
Mg/Ca	2.3	−91.0	2.6±0.8	*Lea et al.* [2000]
Faunal, δ^{18}O	28.4	−158.2	2	*Lee and Slowey* [1999]
Faunal	equatorial eastern Pacific and Atlantic		1 – 6	*Mix et al.* [1999]

[a] For some of the proxies, notably alkenones, additional data exist. Uncertainties represent 1σ error estimates, as given in the cited sources.
[b] South <0.
[c] West <0.

Table 3. Snowline Depression Data From *Porter* [2001][a]

Location	Latitude,[b] deg	Longitude,[c] deg	ΔELA, m
Iztaccíhuatl, Mexico	19.2	−98.6	910
Pico Bolivar, Venezuela	8.5	−71.5	900
Mt. Kinabalu, Borneo	6.1	116.6	905
Nevado del Ruíz, Colombia	4.9	−75.3	1075
Nevado de Santa Isabel, Columbia	4.8	−75.4	1000
Ruenzori, Uganda	0.4	30.0	645
Mt. Kenya, Kenya	−0.2	37.5	873
Antisana, Ecuador	−0.5	−78.1	1045
Chimborazo, Ecuador	−1.4	−77.5	865
Kilimanjaro, Tanzania	−3.1	37.4	830
Cordillera Oriental, Peru	−7.6	−77.3	1063
Cordillera Blanca, Peru	−7.7	−78.0	705

[a] Original sources are cited therein.
[b] South <0.
[c] West <0.

of the mechanisms responsible for climate change, rather than for the constraint of SST variation, given that some climate change, with its associated snowline shift, has occurred. *Albrecht* [1989] has remarked that the effect of aerosols in inhibiting drizzle would tend to increase low cloud fraction as well as cloud albedo, both effects tending to increase the planetary albedo. Such a mechanism might have increased the cooling of an already dusty glacial atmosphere. *Broecker* [2000] has recently discussed the possible effect of dust loading, via these processes, in abrupt climate changes.

13. Summary and Conclusions

[55] The boundary layer model of *Betts and Ridgway* [1989], as modified by *Seager et al.* [2000] to include drizzle from boundary layer clouds, is used to compare the LGM depression of tropical snowlines to a variety of paleotemperature proxies that indicate tropical surface cooling ranging from 1.5 to 6.5 K. The underlying conceptual model involves convergence of boundary layer air into the regions of deep convection, with thermodynamic ascent along an adiabat determined by the equivalent potential temperature, θ_e, of the converging subcloud air. Through the mediation of dynamical processes, the temperature profile set by this deep convection prevails throughout the tropics. The picture is one in which local processes contribute only indirectly to the above-inversion temperature profile, and thus the snowline elevation.

[56] In this framework an SST reduction of 2.8 K proves both necessary and sufficient to produce the observed snowline depression, assuming no significant change in LGM precipitation occurred. The close coupling between SST and θ_e, the equivalent potential temperature of the atmospheric mixed layer, provides a strong constraint on SST once a value for the snowline depression has been introduced. A reduction in precipitation would increase the required reduction in SST by driving snowlines higher with respect to the atmospheric freezing isotherm, with a 20% reduction in precipitation corresponding to an additional SST lowering of 0.4 K. A 20% increase in precipitation would have an effect of similar magnitude but of opposite sign.

[57] While a direct proportionality between changes in latent heat flux at the ocean surface and changes in high mountain precipitation cannot be assumed, a precipitation reduction of 10%, together with an SST lowering of 3.0 K, would be consistent with both the observed snowline depression and such a proportionality.

[58] Some limitations of the class of model employed must be borne in mind. There are no dynamics represented except via parameterization. Cloud fraction, surface winds, ocean heat transport, and other parameters are varied through what are considered reasonable ranges, but the physics of their covariation is not explored. The dependence between cloud fraction and autoconversion would be a likely candidate for such an investigation, and inclusion of an interactive cloud fraction would represent a natural extension of the present model. Again, the clarification of such interactions may tell us more about the processes that produce or maintain the ice-age climate than about glacial SST reduction, once a value for snowline depression is given.

[59] The temperature reconstructions cited, like many paleodata, for the most part represent scattered point measurements and as such place only limited constraints on the reduction in LGM surface temperature in the convecting regions. Since it is likely that SST depression at the LGM was not homogeneous [*Mix et al.*, 2001], local or regional changes in temperature may have occurred that are not reflected in freezing elevation shifts. This differs from the situation aloft, where the small horizontal temperature gradients of the middle troposphere are reflected in the comparative uniformity of snowline elevation changes.

[60] Some reduction of terrestrial temperature relative to SST may be due to the reduced sea level of glacial times, since locations on land would have been shifted upward along the negative lapse rates that begin at the sea surface. Such shifts alone might be expected to account for an offset of ~1 K, approximately half the difference between snowline- and groundwater-derived estimates in Brazil [*Stute et al.*, 1995] but less than one third the difference for the Oman record [*Weyhenmeyer et al.*, 2000]. In addition, this process would not apply to paleotemperature estimates derived from coral geochemistry. Interestingly, *Broccoli* [2000], in an atmosphere-mixed layer ocean model simulation of the LGM, found a mean cooling over tropical land areas just 1 K greater than that over the tropical oceans. The differential cooling was not spatially homogeneous, however.

[61] Spatial variations in tropical cooling may account for all or part of the apparent discrepancy between the snowline depression and the temperature proxy records discussed, but in any event the model simulations suggest a reduction in tropical SST that is intermediate between that indicated by CLIMAP and the 5° or greater cooling indicated by the colder paleotemperature proxies. This reduction is estimated as 2.8–3.2 K, given reductions of high mountain precipitation of 0–20%, or 3.0 K for the scenario in which the change in snowline-driving precipitation is assumed to be proportional to the change in modeled latent heat flux. These SST reductions would apply to an average over the areas of deep convection and, to the extent that changes in these areas reflect changes in mean tropical SST, to the tropics as a whole.

Appendix A: Regression Calculations

[62] In this section we attempt to provide a quantitative estimate of the sensitivity of snowline elevation, or ELA, to changes in

climate parameters, using classical multiple regression analysis. For the problem at hand it is desirable to be able to relate ELA to a small set of climate parameters. Otherwise, a large number of possibly complex assumptions would be required in order to constrain changes in SST, given the observed snowline shifts. We thus consider a limited field of candidate regressor variables. These variables are expressed in gridded form; inferences drawn from the regression would therefore apply to spatially smoothed fields, rather than point microclimates at the sites of individual glaciers. It is determined that just two regressors, based on temperature and precipitation, respectively, capture most of the variance in the ELA data set that represents the criterion variable. Finally, applying the results of the regression to the modern-to-LGM snowline shift amounts to an exchange of spatial and temporal gradients. We discuss the justification for this step later in this section.

[63] Both midlatitude and tropical data are utilized in the regression exercise, even though we are primarily interested in the low-latitude response. There are several reasons for this procedure. In the tropics the dynamic range of both ELA and the atmospheric freezing height, a key predictor, is quite small. Regression relationships derived from this data alone are thus not robust. On the other hand, it can be seen from a plot of ELA against freezing height (Figure A1) that tropical data points lie on the same trend as those in midlatitudes. This is an indication of similarity in response, and indeed, *Hastenrath* [1991] confirms that, like most midlatitude glaciers, those in the tropics lose mass primarily through melting. This would explain the association between ELA and freezing height shown in Figure A1.

[64] Contrastingly, a number of additional snowline data for the very arid subtropical Andes were available [*Hastenrath*, 1971] but were found to lie well above the observed trend, with ELA values as much as 1000 m higher than the freezing elevation. In such a setting it is likely that sublimation, rather than melting, would become the principal term in ablation budgets [*Hastenrath*, 1991]. Aside from questions related to the actual nature of the objects described by the data, this subpopulation is clearly quite different in character than both midlatitude and tropical glaciers and would not be expected to respond in a similar manner to temperature and possibly also precipitation variations. These subtropical data points were consequently excluded from the regression data set. *Wagnon et al.* [1999a, 1999b] found that for a Bolivian glacier at 16°S, partitioning of ablation into sublimation and melting terms was controlled by atmospheric humidity, with dry conditions favoring the former. Over a typical budget year, however, sublimation accounted for less than one fifth of the ablation total, expressed in terms of mass. This is consistent with the observation of *Hastenrath* [1991]. Although the response to precipitation seems to differ between midlatitude and tropical sites (Figure A2), we shall see that the use of indicator, or "dummy," variables in the regression can accommodate this difference. This is not the case with respect to the subtropical sites, however, which showed no discernible response to either temperature or precipitation regressors.

[65] By pooling the data from both midlatitude and tropical sites in a single regression, we gain additional degress of freedom, reducing the error associated with estimates of the regression coefficients [*Neter et al.*, 1996]. Because of the limited dynamic range in the tropical data, and the correspondingly large uncertainty in regression coefficients derived solely from tropical points, this makes a substantial difference in the utility of the regression results.

[66] The regression was carried out assuming that the data comprised two distinct subpopulations, namely, midlatitude and tropical. Inclusion of both subpopulations in the regression carries the implicit assumption that they respond to the same regressors, although identical sensitivities to these regressors are not assumed. The possibility that regression coefficients differ between the two groups is tested by defining a variety of indicator variables and determining whether their inclusion in the regression makes a significant difference in the total variance explained [*Neter et al.*, 1996]. The regression ultimately produces two equations, one corresponding to each subpopulation. Thus the use of a single regression does not imply that changes in midlatitude precipitation or temperature are being used to constrain the reduction in tropical SST. The midlatitude data, rather, are used to improve the estimates of the coefficients in the tropical equation and thus its reliability.

[67] Initially, an assortment of candidate regressors was considered. These included annual and summer means of the atmospheric freezing height and annual, summer, and winter precipitation totals. Summer freezing height was further refined by testing 3-month as well as 6-month averages. The former were taken as JJA or DJF, and the latter were taken as Apr–Sep or Oct–Mar, depending on hemisphere. Seasonal precipitation was computed using the 6-month definitions. In addition, an attempt was made to account for the effect of differential cloud cover by including a cloud radiative forcing data set [*Rossow and Zhang*, 1995] in an annually averaged form. All the climate data used are given on $2.5^\circ \times 2.5^\circ$ grids.

[68] Of the candidate regressors, the one best correlated with ELA was summer freezing height. In preliminary trials that included many subsets of the candidate variables, the 6-month average generally proved somewhat better at explaining variance than the 3-month version, and it alone was ultimately retained. It could be argued that because the seasonal cycle is weak in the tropics, annually averaged temperature would be a more suitable choice. Because of the weak seasonal cycle, however, substitution of the annually averaged temperature for deep tropical sites makes little difference in the regression results. Since at least two of the tropical sites (Meseta volcanoes and eastern Nepal Himalaya; see Table A1) are far enough from the equator to experience at least some seasonality, it was decided, in part for consistency, to simply use the 6-month warm season variant for all sites.

[69] Since the notion of a cold accumulation season is not applicable in the tropics, and since annual and cold-season precipitation are well-correlated for midlatitude sites ($r = 0.96$), annual precipitation was employed as a regressor for all sites. The principal effect of this choice appears in the midlatitude equation, where the sensitivity to precipitation is about one half of what it would have been had winter precipitation been used instead. Since the 6-month winter season is itself a somewhat arbitrary choice, use of annual precipitation allows the regression to decide, in effect, what fraction of the annual precipitation is efficacious in the forcing of snowline changes. When an indicator variable is included, the regression procedure calculates these "efficiency factors" separately for tropics and midlatitudes.

[70] Freezing height was computed for each site from the NCEP-NCAR reanalysis [*Kalnay et al.*, 1996], using a climatology for the period 1950–1979. This period corresponds to the temporal span of the precipitation climatology employed. The NCEP-NCAR atmospheric temperatures, described as "strongly dependent on observations," are based on rawinsonde data and thus are representative of the free atmosphere. However, it is possible that radiosondes released at altitude might still record some influences of the planetary boundary layer, at least in the lower portions of their soundings. We mention this because recent studies in the Andes have found discrepancies between decadal temperature trends in the free atmosphere, as measured by radiosondes and satellites, and those derived from surface observations [*Vuille and Bradley*, 2000]. In a similar vein, *Gaffen et al.* [2000] found that midtropospheric tropical temperatures during the period 1979–1997 cooled, while observations indicate that tropical glaciers were rapidly melting [*Hastenrath and Kruss*, 1992; *Kaser*, 1999]. On the other hand, Figure A1 appears to show a strong correlation between ELA and the free-atmosphere temperature over a wide range. These two sets of observations are not necessarily inconsistent, however.

[71] The temperature data used in the regression and plotted in Figure A1 are 30-year means, taken over the period 1950–1979,

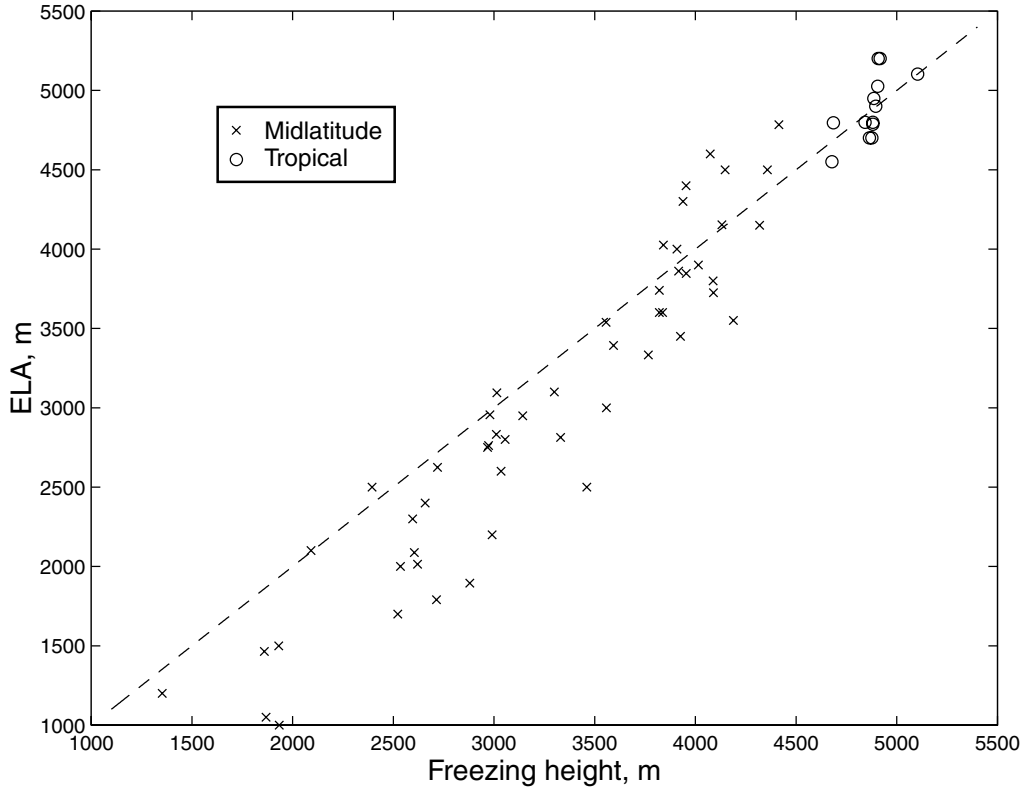

Figure A1. ELA plotted against freezing height. Midlatitude points are shown as crosses; tropical points are shown as circles. Tropical and midlatitude data points lie along the same trend. The dashed line has unit slope; offset of data points from this line indicates departure of ELA values from the local atmospheric (summer) freezing height.

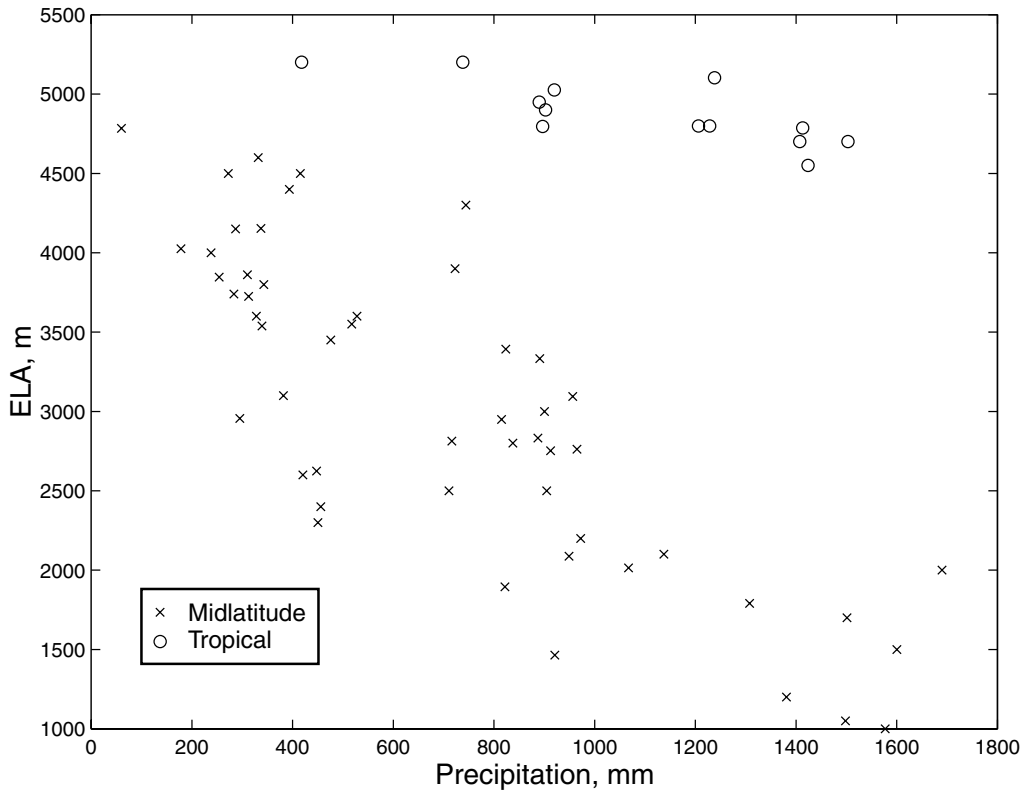

Figure A2. ELA plotted against annual precipitation. As in Figure A1, midlatitude points are shown as crosses, and tropical points are shown as circles. Tropical and midlatitude data points appear to lie on different trends.

Table A1. Glacier and Climate Data Used in the Regression Calculation[a]

Glacier or Location	Latitude,[b] deg	Longitude,[c] deg	ELA	FH	PA	Source
Juneau	58	−134	1050	1868	1498	*Miller* [1961]
Baranof	57	−132	1000	1934	1577	*Péwé* [1975]
Omineca	57	−128	2100	2092	1138	*Pelto* [1992]
Columbia Mountains	54	−123	2500	2395	710	*Pelto* [1992]
Kozelskiy	53	159	1464	1860	921	*Haeberli et al.* [1996]
Purcells	53	−118	2300	2596	450	*Pelto* [1992]
Shuswap	52	−118	2400	2658	456	*Duford and Osborn* [1978]
Peyto	52	−117	2625	2719	448	*Haeberli et al.* [1996]
Place	51	−123	2088	2604	949	*Haeberli et al.* [1996]
Helm	50	−123	2014	2620	1067	*Haeberli et al.* [1996]
Nootka	50	−126	1700	2522	1501	*Halstead* [1968]
Altai	49	86	2956	2980	295	*NSIDC* (1995)[d]
Glacier National Park	49	−114	2600	3035	421	*Flint* [1971]
South Cascade/Glacier Peak	48	−121	1895	2880	821	*Porter* [1964]
Beartooth	47	−113	3100	3299	382	*Pierce* [1978]
Limmern/Plattalva	47	9	2750	2968	912	*Müller* [1977]
Mt. Ranier	47	−122	2200	2990	972	*Porter* [1964]
Sonnblickkees/Wurtenkees	47	13	2762	2973	965	*Haeberli et al.* [1996]
Careser	47	11	3094	3014	957	*Haeberli et al.* [1999]
Gries	47	8	2832	3012	887	*Haeberli et al.* [1999]
Mer de Glace/Glacier d'Argentiére	46	7	2800	3055	837	*Huybrechts et al.* [1989]
Dzhangarskiy Alatau	45	80	3539	3556	339	*NSIDC* (1995)[d]
Glacier Blanc	45	6	2950	3142	815	*Reynaud* [1993]
Jefferson	43	−122	2500	3460	905	*Scott* [1977]
Tsentralniy Tuyuksuyskiy	43	77	3740	3820	283	*Haeberli et al.* [1999]
Urumqihe South Number 1	43	87	4026	3841	178	*Haeberli et al.* [1999]
Wind River	43	−110	3600	3821	328	*Flint* [1971]
Caucasus	43	44	3393	3593	824	*NSIDC* (1995)[d]
Pyrenees	43	0	2813	3331	716	*Serrat and Ventura* [1993]
Tien Shan	43	83	4000	3909	241	*NSIDC* (1995)[d]
Kara−Batkak	42	78	3847	3954	254	*Haeberli et al.* [1996]
Pamiers	42	73	3861	3916	310	*NSIDC* (1995)[d]
Gavur Mountains/Kaçkar/Verçenik	41	40	3333	3766	891	*Kurter* [1991]
Front Range	40	−106	3800	4088	343	*Meierding* [1982]
Mt. Agri	40	44	4300	3938	744	*Kurter* [1991]
Abramov glacier	40	72	4153	4131	337	*Haeberli et al.* [1999]
Mt. Süphan	39	43	3900	4015	723	*Kurter* [1991]
Tarim Basin	39	97	4784	4415	60	*NSIDC* (1995)[d]
Mt. Ericiyes	39	36	3600	3837	528	*Kurter* [1991]
Sabalan	38	48	4500	4147	416	*Ferrigno* [1991]
Bolkar Mountains	38	35	3450	3926	476	*Kurter* [1991]
Buzul/Sat Mountains	37	44	3550	4188	517	*Kurter* [1991]
Sierra Nevada	37	−119	3725	4090	313	*Burbank* [1991]
West Elburz Mountains	37	51	4150	4319	287	*Ferrigno* [1991]
East Elburz Mountains	36	52	4500	4358	272	*Ferrigno* [1991]
East Nepal Himalaya	28	86	5103	5104	1238	*Duncan et al.* [1998]
Meseta volcanoes	19	−99	4800	4843	1228	*White* [1962]
Venezuela	8	−74	4700	4875	1407	*Nogami* [1976]
Colombia	5	−75	4700	4863	1503	*Hastenrath* [1971]
Mt. Kenya	1	38	4796	4685	897	*Haeberli et al.* [1999]
Ruenzori	1	30	4550	4678	1424	*Hastenrath* [1984]
Ecuador	0	−78	4788	4881	1413	*Clapperton* [1987]
Quiches, Marañon, Pelegatos	−8	−77	4800	4882	1206	*Heim* [1948]
Cordillera Blanca	−9	−78	4950	4886	793	*Seltzer* [1990]
Yauricocha/Huancayo	−13	−75	5200	4908	418	*Heim* [1948]
Cordillera de Vilcanota	−14	−71	4900	4895	903	*Newell* [1949]
Cordillera Apolabamba/Cordillera Real	−15	−69	5025	4906	920	*Newell* [1949]
Illampu/Ancohuma/Chearcollo	−16	−69	5200	4916	738	*Troll and Finsterwalder* [1935]
Chicharra/Aconcagua/Ramada	−32	−70	4600	4074	332	*Kuhn* [1911]; *Brüggen* [1950]
Nevado Juncal/Cerro Altar	−33	−70	4400	3953	394	*Brüggen* [1950]
Dumuyo	−36	−73	3000	3558	900	*Nogami* [1976]
North Patagonia	−42	−73	2000	2535	1690	*Nogami* [1976]
Tasman	−44	170	1790	2714	1308	*Chinn* [1991]
Patagonia	−46	−73	1500	1931	1600	*Mercer* [1968]
South Patagonia	−51	−73	1200	1352	1381	*Mercer* [1968]

[a] Sites defined as tropical are those with latitudes between 30°N and 30°S (30 and −30 in the table notation). ELA and FH are given in m; PA is given in mm. Reference dates do not necessarily indicate effective dates of record for the ELA values shown, although secondary sources are referenced directly. ELA data that appear to be given to the nearest meter represent averages either of several regional values or a number of years of observations or both. Climate data are derived from sources mentioned in the text.

[b] South <0.

[c] West <0.

[d] Eurasian Glacier Inventory, 1995, digital data available from The National Snow and Ice Data Center/World Data Center A for Glaciology, nsidc@kryos.colorado.edu, University of Colorado, Boulder, Colorado.

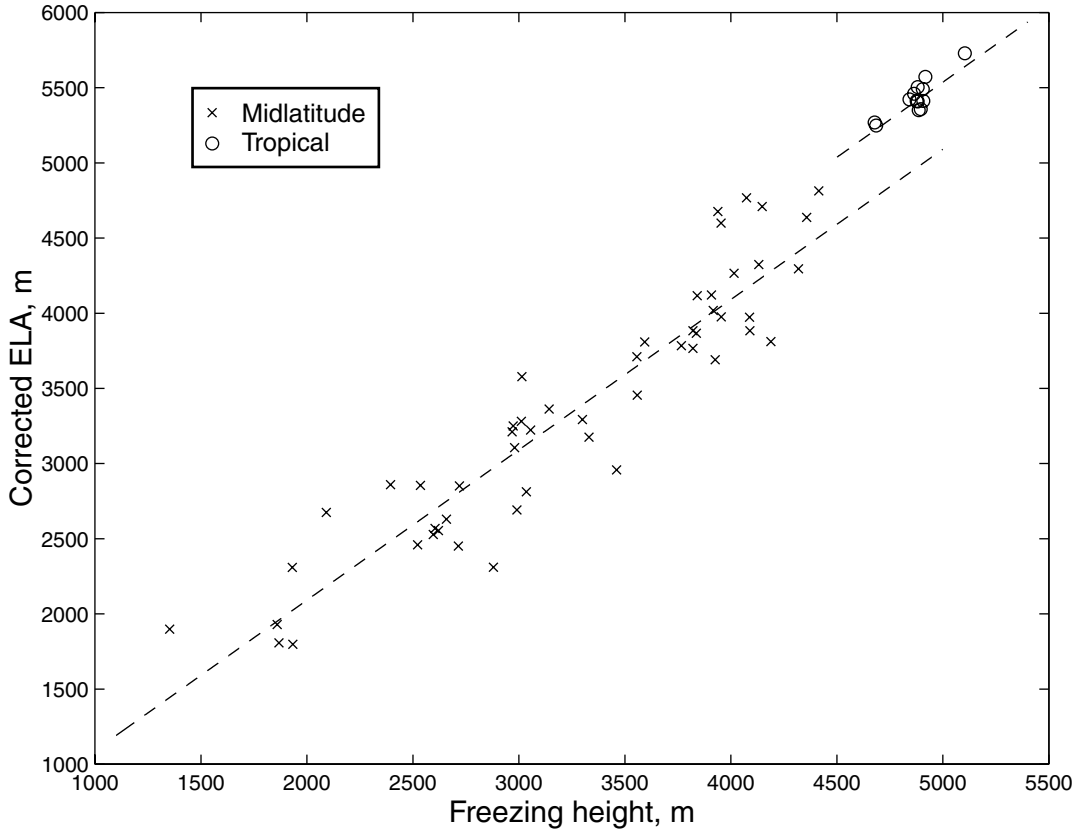

Figure A3. ELA, in this case corrected for the effects of precipitation, plotted against freezing height. Midlatitude points are again shown as crosses, and tropical points are shown as circles. The two dashed lines, both of unit slope, are offset by the difference between constant terms in the midlatitude and tropical regression equations.

during which global temperatures were relatively stable. They are intended to be representative of an approximately stationary state corresponding to the observed distribution of snowlines at around this time. On the other hand, studies such as *Vuille and Bradley* [2000] and *Gaffen et al.* [2000] are focused on transient behavior and record decadal fluctuations that are comparable to, or smaller than, regression error terms. For example, the mean square regression residual for tropical sites is 56 m, about twice the decadal trend in freezing height indicated by *Gaffen et al.* [2000] for the period 1979–1997. Thus, trend differences of this magnitude would probably be absorbed in regression errors, assuming they did not persist for many decades. In this regard it may be worth noting that while *Gaffen et al.* [2000] find a decreasing trend in free-atmosphere freezing height for the period 1979–1997, the trend reported for the period 1960–1997 was positive. Finally, Figure A1 suggests that there is a limit to the offset than can persist between surface and free-atmospheric temperatures and that the latter are ultimately sensed at the surface, if possibly in the presence of distortion attributable to the proximity of the land surface [*Molnar and Emanuel*, 1999]. Beyond these arguments we must assume that any such offsets, if indeed they exist in the long-term mean, did not greatly differe between modern and LGM times, just as the elevation of the land surface itself did not change appreciably during this interval.

[72] In an extended series of tests, the cloud radiative forcing data was found not to reduce variance significantly, either alone or in combination with any other subset of regressors, and it was ultimately dropped from the regression. It is likely that differential cloudiness does play a role, at least in some locations, in forcing snowline deviations. However, the spatial scale of such forcing may be too small to be captured by the gridded data set. Additionally, only 4 years of data were available, so the climatology of this variable may not be well represented.

[73] Annual values for precipitation were taken from the climatology of *Shea* [1986], spanning the years 1950–1979. Data for both freezing height and precipitation were interpolated bilinearly to the locations of the ELA data points. The ELA data themselves were taken from a variety of field reports (see Table A1 for sources) and have a mean observation date of 1960. In some cases, closely neighboring ELA data were averaged, in both position and elevation, to produce a resolution approximating that of the climate data used in the regression. Most of the snowline depression data supplied by *Porter* [2001] are derived from geographic areas, if not specific glaciers, represented in this data set.

[74] When both freezing height and precipitation are included in the regression, a single indicator variable proves sufficient to describe the responses of the two groups, with the resulting equations ($R^2 = 0.95$)

Midlatitudes

$$\mathrm{ELA} = 91 + 1.01\mathrm{FH} - 0.51\mathrm{PA}, \qquad (A1)$$

Tropics

$$\mathrm{ELA} = 537 + 1.01\mathrm{FH} - 0.51\mathrm{PA}. \qquad (A2)$$

In these expressions, ELA and FH (freezing height) are given in meters, and PA (annual precipitation) is given in millimeters. Both the FH and PA coefficients are statistically significant (standard errors are given below).

[75] Inclusion of a multiplicative indicator variable, to distinguish tropical from midlatitude sensitivity to precipitation change, yields the following somewhat different set of equations:

Midlatitudes

$$\mathrm{ELA} = 140 + 1.00\mathrm{FH} - 0.53\mathrm{PA}, \quad (A3)$$

Tropics

$$\mathrm{ELA} = 509 + 1.00\mathrm{FH} - 0.44\mathrm{PA}. \quad (A4)$$

[76] In this case the tropical group does show a reduced sensitivity to precipitation, as suggested by Figure A2. However, the coefficient difference is not statistically significant, or to put it another way, the quality of the data does not permit the resolution of a coefficient difference. In any event, it is helpful to note that even with the inclusion of this dummy variable, the computed tropical precipitation sensitivity is not greatly altered. And since a precise estimate of the effects of precipitation changes is not required for the task at hand, the PA coefficient need not be known to high accuracy in any case. One reason that the coefficient difference does not appear as large as might be expected from Figure A2 is that the effect of freezing height on ELA is not accounted for in this plot. When the plotted ELA is corrected for this effect, the disparity between the two trends is seen to be considerably reduced (not shown).

[77] Figure A3 illustrates the combined effects of both freezing height and precipitation. In this plot, ELA values have been adjusted for the influence of precipitation, using the PA coefficient from (A1) and (A2). The adjusted ELA values are plotted against freezing height, so the influence of the latter can also be seen. What remains, after both freezing height and precipitation are accounted for, is a constant offset between tropical and midlatitude points. This is shown by the two dashed lines, each of unit slope, and is reflected in the differing constant terms in (A1) and (A2). The tropical-midlatitude offset in absolute ELA values may be a consequence of the lack of seasonal temperature contrasts, and thus the longer effective ablation season (essentially 12 months) in the tropics, compared to midlatitudes. It indicates that for identical values of freezing height and precipitation, the average data set ELA in the tropics lies 446 m above the corresponding midlatitude ELA. The small difference between PA coefficients in (A3) and (A4) is not significant at the 0.05 level. Nominally, it expresses a difference in the efficiency with which precipitation variations, as expressed in the gridded data, are processed into snowline elevation changes.

[78] The strong dependence of ELA on freezing height, over a wide range, suggests a justification for the exchange of spatial and temporal gradients, as mentioned earlier. This is simply that the melting point of ice is equally invariant with respect to translation in space and time. Of the two regressors finally retained, FH is by far the more effective at explaining variance in ELA. Rather than attempting to enumerate factors that may have produced differing coefficients in a regression conducted over time, rather than space, we assume, on the basis of the foregoing observation, that their effects are likely to be small compared to the dominant influence of freezing height.

[79] Equation (A2) is the one employed in section 6 to estimate the sensitivity of ELA to changes in precipitation. Standard errors of the FH and PA coefficients are 0.07 and 0.12, respectively.

[80] **Acknowledgments.** We are grateful to Chris Bretherton, Rick Fairbanks, Ray T. Pierrehumbert, Stephen C. Porter, John Shepherd, and Adam Sobel for helpful comments and discussions and to two anonymous reviewers for prodding us to clarify a number of ideas presented herein. Financial support for this research was provided by the National Oceanic and Atmospheric Administration Climate and Global Change Program, grant NA96GP0405, the Climate Dynamics Program of the National Science Foundation, grant ATM97-30546, NOAA grant UCS10P010156283, and NSF grants ATM 9986072 and 9986515. LDEO contribution 6221.

References

Albrecht, B., Aerosols, cloud microphysics and fractional cloudiness, *Science*, *245*, 1227–1230, 1989.

Albrecht, B., Effects of precipitation on the thermodynamic structure of the trade wind boundary layer, *J. Geophys. Res.*, *98*, 7327–7337, 1993.

Baker, P. A., G. O. Seltzer, S. C. Fritz, R. B. Dunbar, M. J. Grove, P. M. Tapla, S. L. Cross, H. D. Rowe, and J. P. Broda, The history of South American tropical precipitation for the past 25,000 years, *Science*, *291*, 640–643, 2000.

Bard, E., Ice age tempertures and geochemistry, *Science*, *284*, 1133–1134, 1999.

Bard, E., F. Rostek, and C. Sonzogni, Interhemispheric synchrony of the last deglaciation inferred from alkenone palaeothermometry, *Nature*, *385*, 707–710, 1997.

Beck, J., R. Edwards, E. Ito, F. Taylor, J. Recy, F. Rougerie, P. Joannot, and C. Henin, Sea-surface temperature from coral skeletal strontium/calcium ratios, *Science*, *257*, 644–647, 1985.

Betts, A. K., Saturation point analysis of moist convective overturning, *J. Atmos. Sci.*, *39*, 1484–1505, 1982.

Betts, A. K., Mixing line analysis of clouds and cloudy boundary layers, *J. Atmos. Sci.*, *42*, 2751–2763, 1985.

Betts, A. K., and W. Ridgway, Climatic equilibrium of the atmospheric convective boundary layer over a tropical ocean, *J. Atmos. Sci.*, *46*, 2621–2641, 1989.

Betts, A. K., and W. Ridgway, Tropical boundary layer equilibrium in the last ice age, *J. Geophys. Res.*, *97*, 2529–2534, 1992.

Broccoli, A., Tropical cooling at the Last Glacial Maximum: An atmosphere-mixed layer ocean model simulation, *J. Clim.*, *13*, 951–976, 2000.

Broecker, W. S., Abrupt climate change: Causal constraints provided by the paleoclimate record, *Earth Sci. Rev.*, *51*, 137–154, 2000.

Brüggen, J., *Fundamentos de la Geología de Chile*, Inst. Geográf. Míl., Santíago, Chile, 1950.

Burbank, D., Late Quaternary snowline reconstructions for the southern and central Sierra Nevada, California and a reassessment of the "Recess Peak" glaciation, *Quat. Res.*, *36*, 294–306, 1991.

Chinn, T. J. H., Glaciers of New Zealand, in *Glaciers of Iryan Jaya, Indonesia and New Zealand: Satellite Image Atlas of Glaciers of the World*, edited by R. Williams Jr. and J. Ferrigno, *U.S. Geol. Surv. Prof. Pap. 1386-H*, H25–H48, 1991.

Clapperton, C. M., Glacial geomorphology, Quaternary glacial sequence and palaeoclimatic inferences in the Equadorian Andes, in *International Geomorphology 1986*, edited by V. Gardiner, pp. 843–870, John Wiley, New York, 1987.

Clement, A., and R. Seager, Climate and the tropical oceans, *J. Clim.*, *12*, 3383–3401, 1999.

Climate: Long-Range Investigation, Mapping, and Prediction (CLIMAP) Project Members, Seasonal reconstruction of the Earth's surface at the Last Glacial Maximum, *Geol. Soc. Am. Map Chart Ser.*, *36*, 1–18, 1981.

Crowley, T. J., CLIMAP SSTs re-revisited, *Clim. Dyn.*, *16*, 240–255, 2000.

Duford, J. M., and G. D. Osborn, Holocene and latest Pleistocene cirque glaciation in the Shuswap highlands, British Columbia, Canada, *Quat. Res.*, *26*, 865–873, 1978.

Duncan, C. C., A. J. Klein, J. G. Masek, and B. L. Isacks, Comparison of late Pleistocene and modern glacier extents in central Nepal based on digital elevation data and satellite imagery, *Quat. Res.*, *49*, 241–254, 1998.

Emanuel, K. A., *Atmospheric Convection*, Oxford Univ. Press, New York, 1994.

Emeis, K.-C., H. Doose, A. C. Mix, and D. D. Schulz-Bull, Alkenone sea-surface temperatures and carbon burial at Site 846 (eastern equatorial Pacific Ocean): The last 1.3 M.Y., in *Proceedings of Ocean Drilling Program, Scientific Results, Leg 138*, edited by N. G. P. et al., pp. 605–613, Ocean Drill. Program, College Station, Tex., 1995.

Fairbanks, R., A 17,000-year glacio-eustatic sea level record: Influence of glacial melting rates on the Younger Dryas event and deep-ocean circulation, *Nature*, *342*, 637–642, 1989.

Farrera, I., et al., Tropical climates at the Last Glacial Maximum: A new synthesis of terrestrial palaeoclimate data, I, Vegetation, lake-levels and geochemistry, *Clim Dyn.*, *15*, 823–856, 1999.

Ferrigno, J. G., Glaciers of Iran, in *Glaciers of the Middle East and Africa: Satellite Image Atlas of Glaciers of the World*, edited by R. Williams Jr. and J. Ferrigno, *U.S. Geol. Surv. Prof. Pap., 1386-G*, G31–G47, 1991.

Fleming, K., P. Johnston, D. Zwartz, U. Yokoyama, K. Lambeck, and

J. Chappell, Refining the eustatic sea-level curve since the Last Glacial Maximum using far- and intermediate-field sites, *Earth Planet. Sci. Lett.*, *163*, 327–342, 1998.
Flint, R. F., *Glacial and Quaternary Geology*, John Wiley, New York, 1971.
Gaffen, D. J., B. D. Santer, J. S. Boyle, J. R. Christy, N. E. Graham, and R. J. Ross, Multidecadal changes in the vertical temperature structure of the tropical troposphere, *Science*, *287*, 1242–1245, 2000.
Gasse, F., Hydrological changes in the African tropics since the Last Glacial Maximum, *Quat. Sci. Rev.*, *19*, 189–211, 2000.
Guilderson, T. P., R. G. Fairbanks, and J. L. Rubenstone, Tropical temperature variations since 20,000 years ago: Modulating inter-hemispheric climate change, *Science*, *263*, 663–665, 1994.
Haeberli, W., M. Hoelzle, and S. Suter (Eds.), *Glacier Mass Balance Bulletin No. 4*, World Glacier Monit. Serv., Zürich, Switzerland, 1996.
Haeberli, W., M. Hoelzle, and R. Frauenfelder (Eds.), *Glacier Mass Balance Bulletin No. 5*, World Glacier Monit. Serv., Zürich, Switzerland, 1999.
Halstead, E. C., The Cowichan ice tongue on Vancouver Island, *Can. J. Earth Sci.*, *5*, 1409–1415, 1968.
Hastenrath, S. L., On the Pleistocene snow-line depression in the arid regions of the South American Andes, *J. Glaciol.*, *10*, 255–267, 1971.
Hastenrath, S. L., *The Glaciers of Equatorial East Africa*, D. Reidel, Norwell, Mass., 1984.
Hastenrath, S., *Climate Dynamics of the Tropics*, Kluwer Acad., Norwell, Mass., 1991.
Hastenrath, S., and P. D. Kruss, The dramatic retreat of Mount Kenya's glaciers between 1963 and 1987: Greenhouse forcing, *Ann. Glaciol.*, *16*, 127–134, 1992.
Hastings, D., A. Russell, and S. Emerson, Foraminiferal magnesium in globeriginoides sacculifer as a paleotemperature proxy, *Paleoceanography*, *13*, 161–169, 1998.
Heim, A., *Wunderland Peru*, Verlag Hans Huber, Bern, 1948.
Held, I. M., and A. Y. Hou, Nonlinear axially symmetric circulations in a nearly inviscid atmosphere, *J. Atmos. Sci.*, *37*, 515–533, 1980.
Hostetler, S. W., and P. U. Clark, Tropical climate at the Last Glacial Maximum inferred from glacier mass-balance modeling, *Science*, *290*, 1747–1750, 2000.
Hostetler, S. W., and A. C. Mix, Reassessment of ice-age cooling of the tropical ocean and atmosphere, *Nature*, *399*, 673–676, 1999.
Huybrechts, P., P. de Nooze, and H. Decleir, Numerical modeling of glacier d'Argentière and its historic front variations, in *Glacier Fluctuations and Climatic Change*, edited by J. Oerlemans, pp. 373–389, Kluwer Acad., Norwell, Mass., 1989.
Kalnay, E., et al., The NCEP/NCAR 40-year reanalysis project, *Bull. Am. Meteorol. Soc.*, *77*, 437–471, 1996.
Kaser, G., A review of the modern fluctuations of tropical glaciers, *Global Planet. Change*, *22*, 93–103, 1999.
Kuhn, F., Beiträge zur Kenntnis der Argentinischen Cordillere zwischen 24 and 26° sudl., *Z. Ges. Erdkunde Berlin*, *46*, 147–172, 1911.
Kurter, A., Glaciers of Turkey, in *Glaciers of the Middle East and Africa: Satellite Image Atlas of Glaciers of the World*, edited by R. Williams Jr. and J. Ferrigno, *U.S. Geol. Surv. Prof. Pap., 1386-G*, G1–G30, 1991.
Lea, D. W., D. K. Pak, and H. J. Spero, Climate impact of late Quaternary equatorial Pacific sea surface temperature variations, *Science*, *289*, 1719–1724, 2000.
Lee, K. E., and N. C. Slowey, Cool surface waters of the subtropical North Pacific Ocean during the last glacial, *Nature*, *397*, 512–514, 1999.
Lindzen, R., and S. Nigam, On the role of sea surface temperature gradients in forcing low-level winds and convergence in the tropics, *J. Atmos. Sci.*, *44*, 2418–2436, 1987.
Lyle, M., F. Prahl, and M. Sparrow, Upwelling and productivity changes inferred from a temperature record in the central equatorial Pacific, *Nature*, *355*, 812–815, 1992.
Meierding, T., Late Pleistocene glacial equilibrium-line altitudes in the Colorado front range: A comparison of methods, *Quat. Res.*, *18*, 289–310, 1982.
Mercer, J. H., Variations of some Patagonia glaciers since the Late Glacial, *Am. J. Sci.*, *266*, 91–109, 1968.
Miller, M. M., A distribution study of abandoned cirques in the Alaska-Canada boundary range, in *Geology of the Arctic*, vol. 1, pp. 831–847, Univ. of Toronto Press, Toronto, Ontario, Canada, 1961.
Mix, A. C., A. E. Morey, and N. G. Pisias, Foraminiferal faunal estimates of paleotemperature: Circumventing the no-analog problem yields cool ice age tropics, *Paleoceanography*, *14*, 350–359, 1999.
Mix, A. C., E. Bard, and R. Schneider, Environmental processes of the ice age: Land, oceans, glaciers (EPILOG), *Quat. Sci. Rev.*, *20*, 627–657, 2001.
Molnar, P., and K. A. Emanuel, Temperature profiles in radiative-convective equilibrium above surfaces at different heights, *J. Geophys. Res.*, *104*, 24,265–24,271, 1999.
Müller, F., *Fluctuations of Glaciers 1970–1975*, vol. 3, Int. Assoc. Hydrol. Sci. and UNESCO, Paris, 1977.
Neter, J., M. H. Kutner, C. J. Nachtsheim, and W. Wasserman, *Applied Linear Statistical Models*, 4th ed., Irwin, Chicago, Ill., 1996.
Newell, N. D., Glaciation of the Titicaca region, *Mem. Geol. Soc. Am.*, *36*, 1949.
Nogami, M., Altitude of the modern snowline and the Pleistocene snowline in the Andes, *Geogr. Rep. 11*, Tokyo Metrop. Univ., Tokyo, 1976.
Ohkouchi, N., K. Kawamura, T. Nakamura, and A. Taira, Small changes in the sea surface temperature during the last 20,000 years: Molecular evidence from the western tropical Pacific, *Geophys. Res. Lett.*, *21*, 2207–2210, 1994.
Pelto, M., Equilibrium line alititude variations with latitude, today and during the late Wisconsin, *Palaeogeogr. Palaeoclimatol Palaeoecol*, *95*, 41–46, 1992.
Péwé, T. L., Quaternary geology of Alaska, *U.S. Geol. Surv. Prof. Pap.*, *834*, 1975.
Pierce, K. L., History and dynamics of glaciation in the northern Yellowstone National Park area, *U.S. Geol. Surv. Prof. Pap.*, *729-f*, 1978.
Pinot, S., G. Ramstein, S. P. Harrison, L. C. Prentice, J. Guiot, M. Stute, and S. Joussaume, Topical paleoclimates at the Last Glacial Maximum: Comparison of Paleoclimate Modeling Intercomparison Project simulations and paleodata, *Clim. Dyn.*, *15*, 857–874, 1999.
Porter, S. C., Composite Pleistocene snowline of the Olympic mountains and the Cascade range, *Geol. Soc. Am. Bull.*, *75*, 477–482, 1964.
Porter, S. C., Snowline depression in the tropics during the last glaciation, *Quat. Sci. Rev.*, *20*, 1067–1091, 2001.
Reynaud, L., The French Alps, in *Glaciers of Europe: Satellite Image Atlas of Glaciers of the World*, edited by R. Williams Jr. and J. Ferrigno, *U.S. Geol. Surv. Prof. Pap., 1386-E*, E23–E36, 1993.
Rind, D., Puzzles from the tropics, *Nature*, *346*, 317–318, 1990.
Rind, D., Latitudinal temperature gradients and climate change, *J. Geophys. Res.*, *103*, 5943–5971, 1998.
Rind, D., and D. Peteet, Terrestrial conditions at the Last Glacial Maximum and CLIMAP sea-surface temperature estimates: Are they consistent?, *Quat. Res.*, *24*, 1–22, 1985.
Rossow, W., and Y.-C. Zhang, Calculation of surface and top of atmosphere radiative fluxes from physical quantities based on ISCCP data sets, 2, Validation and first results, *J. Geophys. Res.*, *100*, 1167–1197, 1995.
Rostek, F., G. Ruhland, F. Bassinot, P. Müller, L. Labeyrie, Y. Lancelot, and E. Bard, Reconstructing sea surface temperature and salinity using $\delta^{18}O$ and alkenone records, *Nature*, *364*, 319–321, 1993.
Schneider, E., Axially symmetric steady-state models of the basic state for instability and climate studies, part II, Nonlinear calculations, *J. Atmos. Sci.*, *34*, 280–296, 1977.
Schubert, W. H., P. E. Ciesielski, C. Lu, and R. H. Johnson, Dynamical adjustment of the trade wind inversion layer, *J. Atmos. Sci.*, *52*, 2941–2952, 1995.
Scott, W. E., Quaternary glaciation and volcanism, Metolius river area, Oregon, *Oreg. Geol. Soc. Am. Bull.*, *88*, 113–124, 1977.
Seager, R., A. Clement, and M. Cane, Glacial cooling in the tropics: Exploring the roles of tropospheric water vapor, surface wind speed and boundary layer processes, *J. Atmos. Sci.*, *57*, 2144–2157, 2000.
Seltzer, G., Recent glacial history and paleoclimate of the Peruvian-Bolivian Andes, *Quat Sci. Rev.*, *9*, 137–152, 1990.
Seltzer, G., D. Rodbell, and S. Burns, Isotopic evidence for late Quaternary climatic change in tropical South America, *Geology*, *28*, 35–38, 2000.
Serrat, D., and J. Ventura, Glaciers of the Pyrenees, Spain and France, in *Glaciers of Continental Europe: Satellite Image Atlas of Glaciers of the World*, edited by R. Williams Jr., and J. Ferrigno, *U.S. Geol. Surv., Prof. Pap., 1386-E*, E49–E61, 1993.
Shea, D., *Climatological Atlas: 1950–1979*, Nat. Cent. for Atmos. Res., Boulder, Colo., 1986.
Sikes, E., and L. Keigwin, Equatorial Atlantic sea surface temperature for the last 30 kyr: A comparison of $U^{K'}_{37}$, $\delta^{18}O$ and foraminiferal assemblage temperature estimates, *Paleoceanography*, *9*, 31–45, 1994.
Sonzogni, C., E. Bard, and F. Rostek, Tropical sea-surface temperatures during the last glacial period: A view based on alkenones in Indian ocean sediments, *Quat. Sci. Rev.*, *17*, 1185–1201, 1998.
Stute, M., M. Forster, H. Frischkorn, A. Serejo, J. Clark, P. Schlosser, W. Broecker, and G. Bonani, Cooling of tropical Brazil (5°C) during the Last Glacial Maximum, *Science*, *269*, 379–383, 1995.
Thompson, L. G., E. Mosley-Thompson, M. E. Davis, P.-N. Lin, K. A. Henderson, J. Cole-Dai, J. F. Bolzan, and K. b. Liu, Late Glacial Stage and Holocene tropical ice core records from Huascarán, Peru, *Science*, *269*, 46–50, 1995.
Thompson, L. G., et al., A 25,000-year tropical climate history from Bolivian ice cores, *Science*, *282*, 1858–1864, 1998.
Trenberth, K. E., and J. M. Caron, Estimates of meridional atmosphere and ocean heat transports, *J. Clim.*, *14*, 3433–3443, 2001.

Trenberth, K. E., J. G. Olsen, and W. G. Large, A global ocean wind stress climatology based on ECMWF analyses, *NCAR Tech. Note NCAR/TN-338+STR*, Nat. Cent. for Atmos. Res., Boulder, Colo., 1989.

Troll, C., and R. Finsterwalder, Die Karten der Cordillera Real und des Talkessels von La Paz, *Petermanns Geogr. Mitt.*, *81*, 393–399, 1935.

Vuille, M., and R. S. Bradley, Mean annual temperature trends and their vertical structure in the tropical Andes, *Geophys. Res. Lett.*, *27*, 3885–3888, 2000.

Wagnon, P., P. Ribstein, B. Francou, and B. Pouyaud, Annual cycle of energy balance of Zongo Glacier, Cordillera Real, Bolivia, *J. Geophys. Res.*, *104*, 3907–3923, 1999a.

Wagnon, P., P. Ribstein, G. Kaser, and P. Berton, Energy balance and runoff seasonality of a Bolivian glacier, *Global Planet. Change*, *22*, 49–58, 1999b.

Wallace, J. M., Effect of deep convection on the regulation of tropical sea-surface temperature, *Nature*, *357*, 230–231, 1992.

Warren, S. G., C. J. Hahn, J. London, R. M. Chervin, and R. L. Jenne, Global distribution of total cloud cover and cloud type amounts over the ocean, *NCAR Tech. Notes NCAR/TN-317+STR, DOE Tech. Note DOE/ER-040*, Carbon Dioxide Res. Div., U.S. Dep. of Energy, Washington, D. C., 1988.

Weyhenmeyer, C., S. Burns, H. Weber, W. Aeschback-Hertig, R. Kipfer, H. Loosli, and A. Matter, Cool glacial temperatures and changes in moisture source recorded in Oman groundwaters, *Science*, *287*, 842–845, 2000.

White, S. E., Late Pleistocene glacial sequence for the west side of Iztaccihuatl, Mexico, *Geol. Soc. Am. Bull.*, *73*, 935–938, 1962.

Xu, K.-M., and K. Emanuel, Is the tropical atmosphere conditionally unstable?, *Mon. Weather Rev.*, *117*, 1471–1479, 1989.

W. S. Broecker, A. M. Greene, and R. Seager, Geochemistry Annex, Lamont-Doherty Earth Observatory of Columbia University, 61 Route 9W, Palisades, NY 10964, USA. (amg@ldeo.columbia.edu)